J Adv Ceram

Review

Design strategies for high entropy materials in water electrolysis: Enhancing activity, stability, and reaction kinetics

Jing Zhang[1], Simiao Sha[1], Jianchun Ni[2], Yanran Wang[2], Yiwei Wu[2], Judy N. Hart[3], Michael Ferry[3], Bin Liu[1,✉], Wenxian Li[4,5,✉]

Cite this article: Zhang J, Sha S, Ni J, et al. *J Adv Ceram* 2025, **14**(10): 9221152. https://doi.org/10.26599/JAC.2025.9221152

ABSTRACT: This review aims to establish general guidelines for designing highly active high-entropy materials (HEMs) with respect to lattice choice, component selection, and samorphological design, leading to the optimization of reaction kinetics and catalytic activity. HEMs have shown superior catalytic performance in hydrogen and oxygen evolution reactions because of their high-entropy structure of multielement random mixing, tailored chemical compositions, and tunable functional characteristics. However, the catalytic applications of HEMs are limited by structural instability, limited catalytic efficiency, and low conductivity, as well as their inherently complex and poorly controlled surface configurations. This review briefly introduces the characteristics of HEMs, highlighting their potential as electrocatalysts, which stems from their unique thermodynamic properties resulting from the collective interactions of multiple elements in the lattice. Then, approaches for enhancing the performance of HEMs are discussed, including composition selection, strain engineering, defect introduction, morphology control, support use, and the role of computational methods, particularly in guiding composition selection. Unlike prior reviews focusing on individual aspects of HEMs, this review systematically integrates computational-guided composition screening, defect engineering, strain modulation, and morphological control with thermodynamic-kinetic stability analysis, offering a holistic design framework that bridges multi-element synergy, surface optimization, and electronic structure tuning for practical electrocatalysis. Additionally, the discussion of stability is grounded in the thermodynamic principles of high entropy and the kinetics of slow diffusion. Finally, insights into challenges and prospects, including *in situ* characterization techniques, emerging computational methods, and scalability, are outlined to guide future advanced design strategies and fabrication technologies.

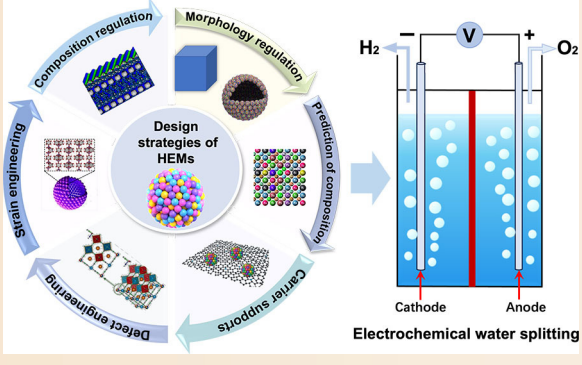

KEYWORDS: hydrogen energy; high-entropy materials ; water splitting; defects; strain; element selection

1 Introduction

With increasing carbon emissions and growing energy consumption, addressing energy sustainability has become increasingly critical [1–3]. Global energy consumption, which is currently dominated by fossil fuels (95%), is projected to quadruple to 28 TW by 2050, equivalent to 20 billion tons of oil annually [4–6]. The greenhouse gas (GHG) emissions from fossil fuel consumption are causing severe environmental challenges, including global warming, glacier melting, and rising sea levels [7–9]. Given the concerns about the exhaustion of fossil fuels and the accompanying environmental harm, renewable energy-driven water electrolysis for hydrogen generation offers a promising solution [10–12]. Hydrogen (H_2), with an energy density of ~142 MJ·kg^{-1}, holds great potential for decarbonizing transportation, electricity production, and energy storage, particularly when it is produced by environmentally-friendly and sustainable methods [13–15].

Water splitting involves two distinct half-reactions—the hydrogen evolution reaction (HER) and the oxygen evolution reaction (OER) [16,17]. The HER follows a two-electron transfer mechanism [18,19]. In contrast, the OER is a significantly more intricate electrochemical process, requiring the transfer of four electrons coupled with four protons. Thermodynamically, water splitting requires overcoming intrinsic energy barriers associated

[1] School of Materials Science and Engineering, Shanghai University, Shanghai 200444, China. [2] Baowu Clean Energy Co., Ltd., Shanghai 201900, China. [3] School of Materials Science and Engineering, University of New South Wales, New South Wales 2052, Australia. [4] School of Chemical Engineering, University of New South Wales, New South Wales 2052, Australia. [5] Australian Research Council Centre of Excellence for Carbon Science and Innovation, University of New South Wales, New South Wales 2052, Australia.

✉ Corresponding authors. E-mail: B. Liu, binliu@shu.edu.cn; W. Li, wenxian.li1@unsw.edu.au

Received: June 5, 2025; Revised: July 22, 2025; Accepted: August 14, 2025

with the breaking and formation of chemical bonds in the HER and OER, with a well-defined minimum theoretical voltage of 1.23 V under standard conditions [20,21]. In practical applications, however, an additional energy input (termed overpotential η) is required to drive the reaction at an appreciable rate [22,23]. The overpotential arises primarily from kinetic limitations, which are governed by the sluggish reaction pathways and the adsorption/desorption of intermediates on the electrode surfaces [24]. Central to understanding and improving catalytic performance is reaction kinetics-the study of the rates of chemical reactions and the factors influencing them [25]. These challenges are fundamentally linked to the operational framework of electrocatalytic water splitting, which relies on two critical interdependent processes: liquid-phase mass transfer involving the adsorption/desorption of substrates and reactive intermediates, and electron transfer that occurs at the electrode interfaces [26]. The performance of both processes is deeply governed by the intrinsic characteristics of the electrochemical catalysts [27,28]. Thus, pioneering research into highly effective electrocatalysts is essential for efficiently converting electrical energy into hydrogen energy by water splitting [29–31].

Of particular importance is the interaction strength between the catalyst surface and the reaction intermediates, which significantly influences catalytic performance [32,33]. The reaction mechanisms for both OER and HER involve multiple reaction intermediates, including *OH, *OOH, and *H [34–36], and it is necessary to consider the adsorption behavior of these intermediates when designing catalysts [37,38]. Adsorption strength plays a particularly crucial role in determining the interaction between intermediates and the catalyst surface. To develop efficient electrocatalytic materials, optimization of this adsorption strength as well as factors such as an extensive specific surface area, enhanced porosity, well-optimized distribution of active sites, and superior charge transfer capability, should be prioritized [39–41]. Currently, Pt-based and RuO_2 catalysts remain rhe representative materials for high performance in the HER and OER and have been widely used because of their remarkable catalytic performance [42–44]. However, limited resources, high cost, and poor long-term stability pose significant challenges for industrial applications of these catalytic materials [45,46].

Combining multiple elements within a single material offers a powerful strategy for precisely tuning catalytic properties, such as activity and stability [47]. However, this approach faces limitations due to thermodynamic immiscibility between certain elements, which can prevent the formation of uniform phases or alloys [48]. Immiscibility is not inherently problematic for catalysts such as Pt or RuO_2, which function effectively as standalone or composite materials [49]. However, it becomes a significant challenge when synergistic interactions between immiscible components are needed. For example, in advanced bimetallic or multioxide systems, phase segregation can degrade performance by reducing active-site accessibility or destabilizing interfaces [50].

Recently, high-entropy materials (HEMs) have gained significant attention as promising catalysts for water electrolysis because the high-entropy structure of HEMs overcomes immiscibility among elements, enabling precise compositional control and facilitating the optimization of catalytic properties [51,52]. The random arrangement of multiple elements in HEMs induces a significantly disordered atomic structure within a shared lattice matrix due to the enormous configurational entropy (ΔS_{conf}) and complicated local atomic environments [53,54]. HEMs are further distinguished by other remarkable characteristics, including lattice distortion, sluggish diffusion, and the intriguing "cocktail" effect, positioning them as exceptional prospects for catalytic applications [55]. The lattice distortion arising from disparities in atomic size places HEMs in a thermodynamically non-equilibrium state, effectively lowering the energy barriers associated with molecular adsorption, activation, and conversion during electrocatalytic reactions [56,57]. Moreover, the highly disordered structure and irregular elemental distribution inherent to HEMs generate abundant surface vacancies and other defects and coordinatively unsaturated sites. This configuration provides substantially more active centers compared to single-element catalysts do, thereby improving water-splitting efficiency [58,59]. HEMs also facilitate lattice oxygen activation, effectively lowering the thermodynamic barrier for water oxidation [60,61]. In addition to enhancing surface activity, the intrinsic high entropy combined with slow diffusion dynamics endows HEMs with exceptional thermal stability, ensuring their durability under diverse reaction environments, including elevated temperatures, oxidative atmospheres, and acidic or alkaline conditions [62,63]. In addition, the cocktail effect arising from multi-element atomic-level mixing in HEMs facilitates electronic interactions, creating multiple active sites and enabling near-continuous tuning and hence optimization of adsorption energies [64,65]. The optimization of the adsorption energy (E_{ad}), a key factor influencing catalytic performance, enables the catalyst to achieve a balance between reactant binding and product release [66]. This balance is commonly represented by the "volcano plot", which describes the relationship between catalytic activity and adsorption energy, where activity shows a volcano-like trend: too strong or too weak adsorption hinders activity, with the peak representing the optimal balance for maximum catalytic performance [67,68]. In summary, the distinctive features of HEMs contribute to the ability to tune the adsorption and desorption of intermediates, along with charge transfer, offering promising potential to reduce the excessive overpotentials associated with thermodynamic energy barriers in water electrolysis [69]. These inherent properties collectively underpin the exceptional catalytic tunability of HEMs. The design of HEMs is intrinsically tied to the core principles of reaction kinetics [70]. The extensive compositional space afforded by HEMs presents an unprecedented opportunity to tailor catalyst surfaces at the atomic level. Such tailoring aims to directly modulate the kinetics of catalytic reactions by [71]: (i) optimizing the adsorption energies of key intermediates to reduce the activation barrier of the rate-determining step (RDS), (ii) creating synergistic multi-functional sites that enable alternative, lower-energy reaction pathways, (iii) stabilizing active sites against reconstruction under reaction conditions to maintain favorable kinetics over time, and (iv) modulating the electronic structure to facilitate specific electron transfer steps crucial to the reaction mechanism. Therefore, the rational design of HEMs is not merely compositional exploration. It is fundamentally an exercise in kinetic engineering, which involves the manipulation of the energy landscape of surface reactions to achieve superior catalytic performance.

In recent years, multiple types of HEMs have covered a wide range of chemical compositions, positioning them as formidable contenders as water electrolysis catalysts. Since 2019, substantial advancements have been made in the development of HEMs for HER and OER, which have demonstrated remarkable activity (Fig. 1(a)). A number of high-entropy nanomaterials, such as high-entropy alloys (e.g., MnFeCoNi and MnFeCoNiCu) [72,73], high-entropy phosphides (e.g., NiCoFeMnCrP) [74], high-entropy sulfides (e.g., CoZnCdCuMnS and $FeCoNiMnMoS_x$) [75,76], high-entropy oxides (e.g., $Fe_{0.27}$ $Ni_{0.35}Co_{0.24}Cr_{0.10}Mn_{0.04}O_{3-\delta}$) [77], high-entropy fluorides and high-entropy carbides, etc., have garnered

significant attention. Collectively, these different classes of HEMs are referred to high-entropy compounds [78,79].

The growing interest in HEMs for electrocatalysis is evident in both research output and application diversity. As shown in Fig. 1(b), the number of published articles on HEMs in HER and OER applications has steadily increased, from 15 in 2021 to 36 projected for 2024, highlighting a rapid expansion in scientific attention. Furthermore, the application distribution of HEMs over the past five years reveals that water electrolysis dominates at 66%, followed by degradation processes (12%) and oxidative desulfurization (10%), with smaller contributions from CO reduction, lithium-sulfur batteries, and other fields (Fig. 1(c)). This demonstrates the versatility of HEMs and their significant potential in advancing sustainable energy technologies. These trends reflect the burgeoning recognition of HEMs as promising candidates in various electrocatalytic applications.

The biggest challenge faced by HEMs as electrocatalysts is understanding the intricate correlation between their complex structural features and electrochemical performance because many elements are introduced into HEMs and the entangled electronic effects increase the challenges in finding and hence optimizing the genuine active sites [80–82]. However, the catalytic applications of HEMs are critically constrained by not only their activity but also stability [83,84]. Consequently, striking an optimal balance between catalytic performance and structural stability has become a central focus of current research [85–91].

Several recent reviews have summarized the design and development of HEMs and have given overviews of their applications in electrocatalysis [71,92,93]. These previous reviews on HEMs have primarily focused on synthesis methods, structural characterization, or their broad applications in electrocatalysis. In contrast, this review presents a pioneering and comprehensive framework that systematically integrates mechanistic insights, design strategies, and stability optimization approaches—specifically tailored for HEMs in water electrolysis. To provide actionable insights for the rational design of high-performance catalytic materials, we consolidate recent progress in HEM design strategies within the context of water electrolysis. Our focus lies in

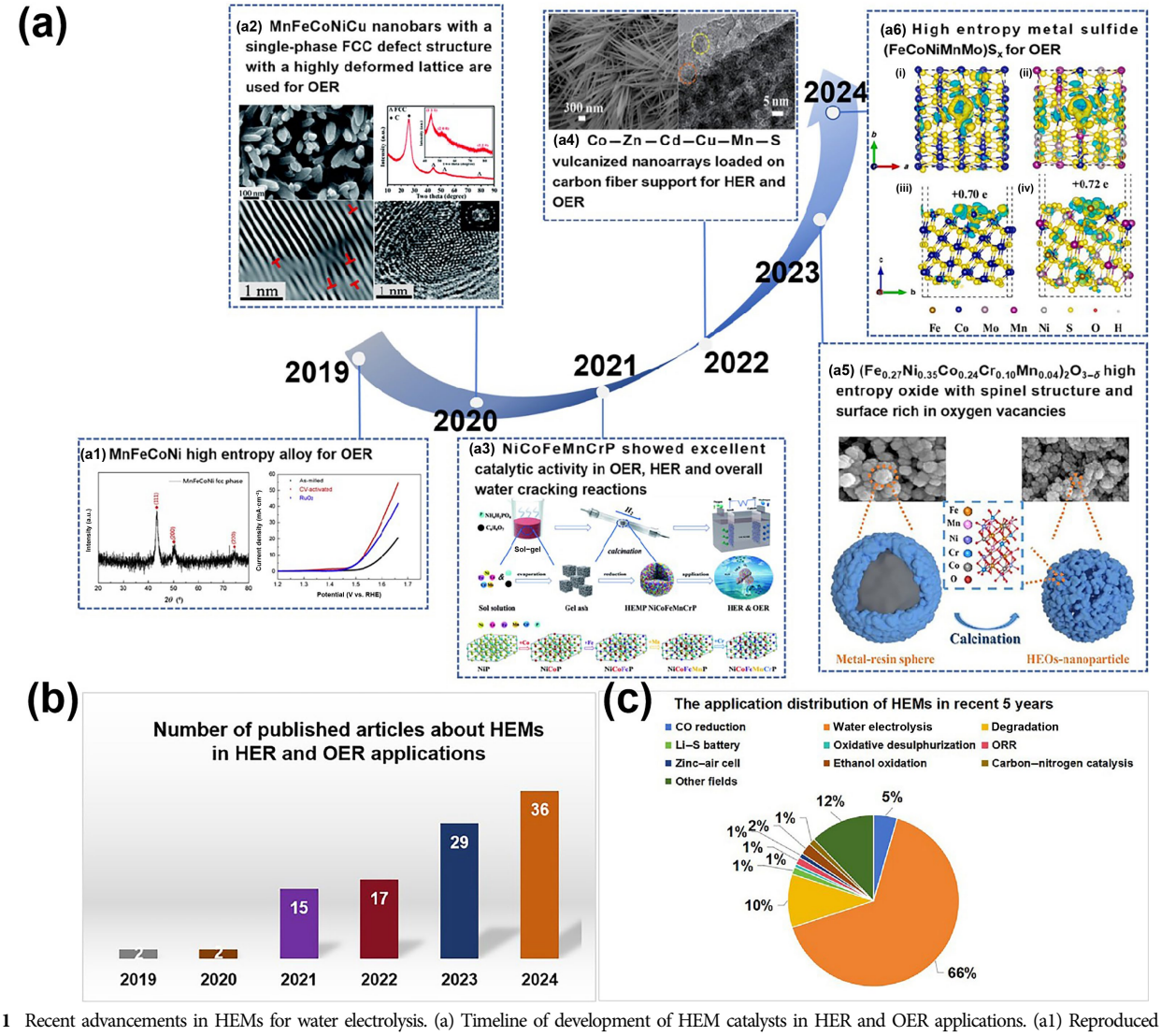

Fig. 1 Recent advancements in HEMs for water electrolysis. (a) Timeline of development of HEM catalysts in HER and OER applications. (a1) Reproduced with permission from Ref. [72], © Elsevier B.V. 2019. (a2) Reproduced with permission from Ref. [73], © Royal Society of Chemistry 2020. (a3) Reproduced with permission from Ref. [74], © Royal Society of Chemistry 2021. (a4) Reproduced with permission from Ref. [75], © Tsinghua University Press 2022. (a5) Reproduced with permission from Ref. [77], © Elsevier B.V. 2023. (a6) Reproduced with permission from Ref. [76], © Hydrogen Energy Publications LLC. 2024. (b) Statistics on the number of published research articles on HEMs in water electrolysis since 2019, sourced from the Web of Science. (c) Statistical data on application of HEM catalysts over past five years, derived from the Web of Science.

清華大学出版社 Tsinghua University Press | SciOpen

elucidating how to generate reaction sites with high intrinsic activity while increasing the overall number of active sites. These strategies are essential for developing catalysts with superior efficiency.

The design strategies covered in this review include compositional tuning, strain and defect engineering, morphology control, metal-support interaction optimization, and computational prediction of ideal elemental combinations. These strategies are examined in the context of enhancing electrocatalytic activity and stability. Compared with prior reviews, our analysis integrates theoretical insights and experimental practices, emphasizing how multi-element synergy, d-band center modulation, lattice distortion, and morphological engineering collectively govern catalytic behavior. We also introduce an in-depth discussion on leveraging computational tools to predict optimal elemental configurations and electronic structures, strengthening the connection between simulation and experimental validation. The core objectives of this review are to: (i) establish a clear and robust link between mechanistic studies and catalyst design principles; (ii) highlight design strategies guided by current research advancements; (iii) analyze how morphology, electronic structure, and conductivity affect catalytic performance; and (iv) design promising HEMs with high activity and stability for practical application. We place special emphasis on the often-overlooked activity-stability trade-off—an essential but underexplored factor in HEM development. By addressing this and other unresolved challenges, this review not only enhances understanding of HEM behavior in water electrolysis but also lays the groundwork for future innovations in sustainable energy technologies.

2 Theoretical concept and unique properties of HEMs

2.1 Definition of HEMs

The general concept of HEMs was originally introduced in 2004 in two independent studies by Yeh *et al.* [51] and Cantor *et al.* [52]. Since their inception, HEMs have been rapidly developed and widely regarded as groundbreaking innovations in the field of multicomponent alloy systems. From the perspective of composition, high entropy alloys (HEAs) are considered alloys that incorporate a minimum of five essential elements, with each element being present in the concentration range of 5–35 at% [90,94]. However, this compositional criterion alone is insufficient for reliably predicting the formation of a single-phase solid solution in a multi-element alloy that meets the definition of a HEM [53]. ΔS_{conf} refers to the entropy arising from the number of distinct atomic arrangements possible within a disordered crystalline solid. HEMs stabilize single-phase solid solutions and can influence their catalytic behavior [94]. Thus, ΔS_{conf} is employed to account for the contributions of different elements to the entropy of HEMs (Eq. (1)):

$$\Delta S_{conf} = -R\sum_{i=1}^{n}\chi_i \ln \chi_i \quad (1)$$

where R represents the universal gas constant, and χ_i denotes the mole fraction of the ith component. In statistical thermodynamics, entropy tends to increase proportionally with the number of microscopic states and components in a system [94]. Configuration entropy is typically the dominant factor in determining the mixing entropy of a system, and configurational entropy attains its maximum value when all components exist in equal atomic fractions (i.e., equimolar). In this case, the configurational entropy per mole can be expressed as Eq. (2) [55]:

$$\Delta S_{conf} = R\ln n \quad (2)$$

where n represents the number of components. Yeh and colleagues classified alloys into three distinct classes according to their ideal molar configurational entropy: low entropy ($S_{conf} < 0.69R$), medium entropy ($0.69R < S_{conf} < 1.6R$), and high entropy ($S_{conf} \geq 1.6R$) (Fig. 2(a)) [51]. Achieving $S_{conf} \geq 1.6R$ requires the inclusion of five or more elements with nearly equal atomic proportions [95], leading to the definition of HEAs given above. With the progressive advancements in alloy research, HEAs have been further categorized into two generations [96]. The original definition of HEAs, which mandated strict compositional constraints, was later deemed overly restrictive. To address this limitation, a broader definition was introduced, encompassing non-equimolar, dual, or multiphase structures, as well as systems containing a minimum of only four principal elements [97].

Within the high-entropy principle, S_{conf} is determined exclusively by the number of constituent elements, establishing a balance between the mixing enthalpy (ΔH_{mix}) and S_{mix} as described by the Gibbs–Helmholtz equation (Eq. (3)) [98]:

$$\Delta G_{mix} = \Delta H_{mix} - T\Delta S_{mix} \quad (3)$$

When the thermal contribution from $T\Delta S_{mix}$ balances or surpasses ΔH_{mix}, the crystal structure achieves entropy stabilization, resulting in enhanced compound stability, as greater configurational entropy drives ΔG_{mix} to be negative [55]. Thus, the remarkable structural diversity enabled by multiple element combinations in HEAs results in the creation of stable single-phase solid solutions. These solutions exhibit a variety of crystal structures, such as face-centered cubic (FCC), body-centered cubic (BCC), hexagonal close-packed (HCP), and Laves phase (Fig. 2(b)) [95].

2.2 Development of HEMs

Since Rost *et al.* [99] initially introduced high-entropy oxide ceramics exhibiting a single-phase rock-salt structure, specifically $(Mg_{0.2}Co_{0.2}Ni_{0.2}Cu_{0.2}Zn_{0.2})O$, in 2015, the concept of entropy stabilization has been successfully transferred from alloys to multicomponent oxides, marking the advent of high-entropy ceramics (HECs). The molar configurational entropy of ceramic materials can be calculated via Eq. (4):

$$\Delta S_{conf} = -R\left[\left(\sum_{i=1}^{n} x_i \ln x_i\right)_{\text{cation-site}} + \left(\sum_{j=1}^{m} x_j \ln x_j\right)_{\text{anion-site}}\right] \quad (4)$$

where χ_i and χ_j denote the mole fractions of the elements occupying the cationic and anionic sites, respectively.

Single-phase HECs with rock–salt structures are the most extensively studied and exhibit remarkable structural and compositional flexibility [100], but the term "high entropy" has been expanded to cover a diverse array of materials and nanostructures encompassing oxides, nitrides, and carbides [101,102]. According to its original definition, numerous compounds composed of multiple equal molar components have been developed beyond HEAs, which are collectively referred to as HEMs [99,100]. These compounds include oxides (HEOs) [103], carbides, nitrides, borides (which are collectively categorized as HECs) [104], hydroxides, selenides [75], coordination compounds [105], salts [106], and others. Furthermore, the concept has been

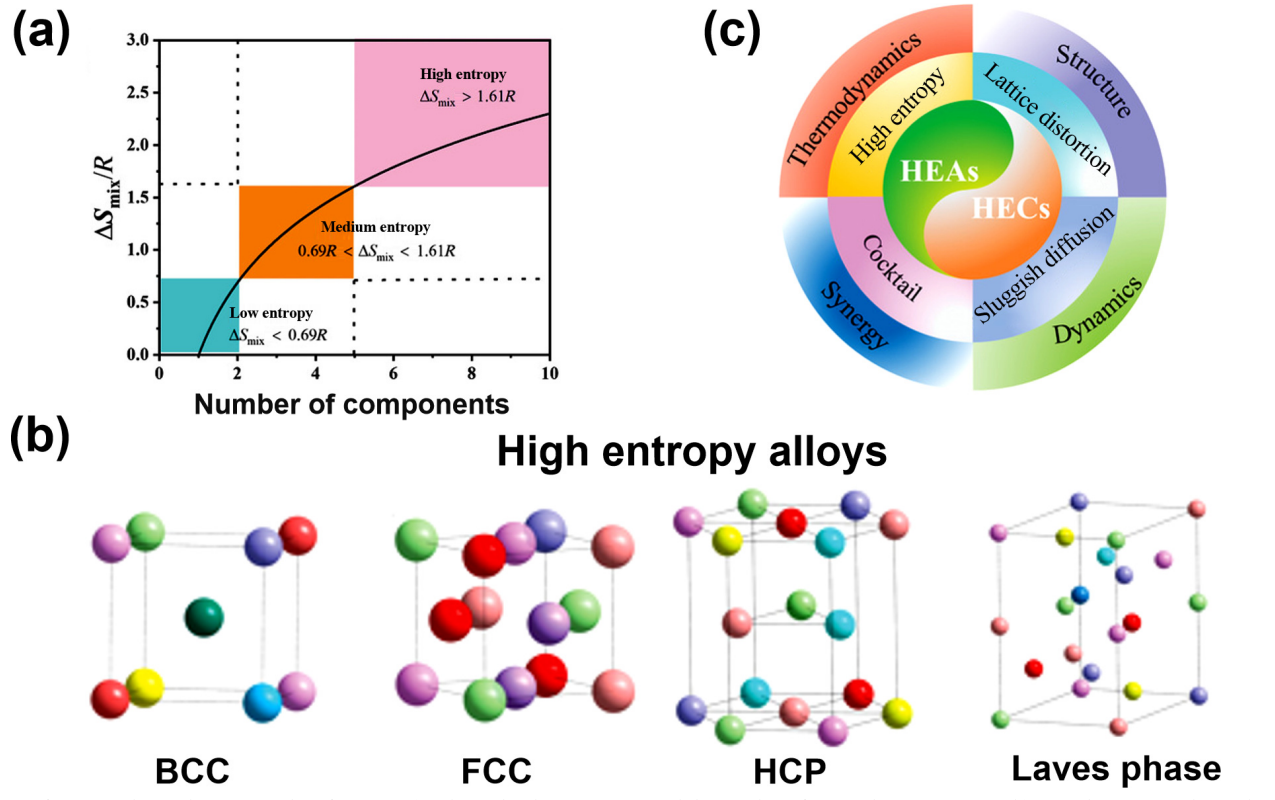

Fig. 2 Definition and crystal structure atlas of HEMs. (a) Relationship between ΔS_{mix} and the number of equimolar components. (b) Crystal structures observed in HEAs. (c) A schematic illustration highlighting the distinctive characteristics of HEMs. Reproduced with permission from Ref. [71], © Wiley-VCH GmbH 2022.

extended to amorphous oxides, metallic glasses, and intermetallic compounds, broadening the scope of HEMs [71].

2.3 Potential of HEMs for electrocatalysis

The critical factors in designing high-performance electrocatalysts are activity and stability [107]. HEMs, because of the varied atomic radii of their multiple components, exhibit unique characteristics of high entropy, lattice distortion, slow diffusion, and the "cocktail" effect. These characteristics, illustrated in Fig. 2(c), endow HEMs with exceptional functions in water-splitting electrocatalysis [62,108]:

(i) The high-entropy effect enhances thermodynamic stability by increasing ΔS_{mix} associated with the high number of components, promoting the establishment of a stable high-entropy system. Consequently, this effect enables HEM catalysts to exhibit surprising durability [109].

(ii) Lattice distortion arises from disparities in atomic sizes and electron distributions among the components, leading to random site occupation and a state of thermodynamic non-equilibrium. This structural distortion, while increasing the intrinsic potential energy of HEMs, significantly reduces the activation energy required for catalytic reactions by optimizing the electronic structure of the active sites [110]. Additionally, tensile lattice strain causes an upward shift in the d-band center, strengthening reactant (O_2/H_2) adsorption. In contrast, compressive strain lowers the d-band position, which weakens interactions with adsorbates during the OER and HER processes [111]. Furthermore, defects caused by lattice distortion can enhance surface adsorption, accelerate reaction kinetics, and reduce the energy of reaction intermediates, collectively improving the water-splitting efficiency of HEMs [68,112].

(iii) From a dynamic perspective, the inherently sluggish diffusion within the lattice inhibits the aggregation of HEMs, which helps mitigate structural degradation under prolonged electrochemical operation. Thus, the disordered or nanoscale configurations provide sustained exposure of active sites, thereby improving long-term catalytic durability [94].

(iv) The "cocktail effect" emerges from the synergistic interactions among various components. Research indicates the performance of HEMs is not merely the sum of individual component properties but is instead unpredictable and often superior. Additionally, the cocktail effect arising from atomic-level multi-element mixing introduces a dynamic electronic environment, offering abundant active sites and enabling near-continuous modulation of adsorption energies [71,113].

On the basis of these unique features, HEMs have emerged as highly promising candidates in the pursuit of efficient catalysts.

3 Design strategies for enhanced the electrochemical activity

HEMs, which leverage the diverse atomic radii and electron configurations of their multicomponent systems, exhibit unique characteristics such as exceptional thermal stability, synergistically tuned electronic structure, and abundant active surface sites [114]. It is critical to consider several aspects, such as morphology, particle size, composition, electronegativity differences between components, the presence of defects, catalyst support, prediction of element combinations via theoretical calculations and electronic structure to attain better electrocatalytic activity and stability [115,116]. Several innovative strategies have successfully led to effective and stable HEM catalysts [117]. These strategies include (i) engineering the catalyst morphology, nanoparticle size, and shape through the fabrication of highly porous [118], hollow or small particle structures to generate many accessible active sites [119–121]; (ii) tailoring the composition to adjust the electronic structure [122–124]; (iii) engineering strong support-particle interactions [125]; and (iv) screening and determining the optimal

combination of elements in HEMs via computational tools [126]. Understanding the intricate relationship between structural attributes and electrocatalytic performance is essential for designing advanced electrocatalysts with tailored physical and chemical properties [127]. The materials, optimization strategies, and HER/OER performance of the HEM-based catalysts reported in recent references are summarized in Table 1. From the data presented, it is evident that optimization strategies for enhancing the activity of HEMs primarily focus on two key aspects: microstructure design, including morphology control, and electronic structure control, mainly from the perspectives of doping, composition tuning, and defect engineering. Of the two approaches, electronic regulation is more conducive to stimulating the active centers of catalytic materials, providing more active sites to promote water splitting.

While traditional noble metal catalysts such as Pt/N–$CoWO_3$ and Ir@Co_3O_4 (Table 2) represent the current performance benchmarks for HER and OER under acidic/alkaline conditions, respectively, HEM catalysts exhibit superior potential. Owing to their inherent unique multicomponent synergistic effects, HEMs outperform conventional noble metal-based catalysts in regulating active sites, structural stability, and cost-effectiveness, with HER and OER performances even exceeding those of traditional benchmarks. Future efforts should therefore focus on an in-depth understanding of high-entropy surface active sites, the development of scalable synthesis techniques, and the enhancement of stability under industrial-level current densities.

3.1 Composition regulation

3.1.1 *Crystal structure effect*

Generally, different crystal structures significantly influence the activity of catalysts, mainly because activity is often influenced by the atomic structure within the lattice, and the interactions between atoms lead to new collective behaviors [68]. Since compositional tuning directly modifies the atomic arrangement and bonding environment, it inherently influences the crystal structure. Furthermore, different crystal phases have different surface atomic configurations and coordination, which are crucial in determining surface energy and catalytic performance [138].

Compared with their binary or ternary counterparts, HEMs exhibit a distinct phase evolution behavior [144]. In binary and ternary alloys, the compositional elements generally exhibit significant immiscibility, leading to the formation of phase-separated structures or intermetallic compounds. This phenomenon restricts the precise modulation of the composition ratio, thereby limiting the optimization of catalytic performance [62]. In contrast, the higher configuration entropy of HEMs promotes the alloying process and stabilizes a uniform single-phase or ideal solid-solution structure [145].

Table 1 Materials, optimization strategies, and HER and OER performance of HEM-based catalysts reported in recent references

Material	Optimization strategy	η_{HER} (mV) at 10 mA·cm^{-2}	Tafel slope (mV·dec^{-1})	η_{OER} (mV) at 10 mA·cm^{-2}	Tafel slope (mV·dec^{-1})	Electrolyte	Ref.
PtCoMoPdRh NFs	Electronic structure	16.5	26.8	—	—	1.0 M KOH	[45]
$Pt_4FeCoCuNi$	Electronic structure	20	31	—	—	1.0 M KOH	[128]
$Pt_{28}Mo_6Pd_{28}Rh_{27}Ni_{15}$	Electronic structure	9.7	25.9	—	—	1.0 M KOH	[129]
ZnNiCoIrMn	Electronic structure	50	30.6	237	46	0.1 M $HClO_4$	[130]
FeCoNiMnRu	Electronegativity difference	71	67.4	308	61.3	1.0 M KOH	[108]
$Co_{0.6}(VMnNiZn)_{0.4}PS_3$	Doping	65.9	65.5	—	—	1.0 M KOH	[54]
P_x–$Ni_{30}Co_{30}Fe_{10}Cr_{10}Al_{18}W_2$	Doping	70	32.6	251	41.3	1.0 M KOH	[131]
PdPtRhIrCu	Defect	15	37	—	—	1.0 M KOH	[110]
$(FeCoNiB_{0.75})_{97}Pt_3$	Defect	104	—	301	—	1.0 M KOH	[132]
NiCoFeMoMn	Morphology control	150	29	243	37	1.0 M KOH	[133]
PtPdRhRuCu	Morphology control	10	87	—	—	1.0 M KOH	[134]
IrFeCoNiCu	Morphology control	—	—	302	58	0.1 M $HClO_4$	[135]
FeCoNiCu	Morphology control	42.2	31.7	—	—	1.0 M KOH	[136]
FeCoNiRu	Morphology control	40	84	243	45	1.0 M KOH	[137]
$Pd_{20}Pt_{20}Cu_{20}Ni_{20}P_{20}$	Morphology control	35.4	34.2	—	—	0.5 M H_2SO_4	[138]
FeCoNiIrRu	Composition regulation	—	—	241	—	0.5 M H_2SO_4	[139]
FeCoNiAlTi	Composition regulation	88.2	40.1	—	—	1.0 M KOH	[140]
$(CrFeCoNi)_{97}O_3$	Composition regulation	—	—	196	29	1.0 M KOH	[141]
CuAlNiMoFe	Crystal structure	183	60	—	—	1.0 M KOH	[87]
FeCoNiCuPd	crystal structure	29	47.2	194	39.8	1.0 M KOH	[142]
PdMoGaInNi	Theoretical prediction	13	—	—	—	0.5 M H_2SO_4	[143]

Table 2 Current best-performing HER and OER catalysts under alkaline and acidic conditions

Reaction	Condition	Best catalyst	Performance	Optimization strategy	Ref.
HER	Alkaline	Ir–Ru@C	13 mV at 10 mA·cm^{-2}	Bimetallic electronic synergy	[42]
	Acidic	Pt/WO_{3-x}	2.8 mV at 10 mA·cm^{-2}	Heterogeneous interfaces	[43]
OER	Alkaline	Au/NiFe-LDH	209 mV at 10 mA·cm^{-2}	Single-atom modification	[12]
	Acidic	Ir/Co_3O_4	248 mV at 10 mA·cm^{-2}	Surface optimization	[14]

The FCC crystal structure plays a pivotal role in enhancing the catalytic performance of HEMs, primarily through its unique atomic arrangement and surface characteristics [109]. As evidenced by Chang *et al.*'s [146] comparative study of three FCC-structured catalysts (H-FeCoNiMn, H-FeCoNiW, and H-FeCoNiMnW), the H-FeCoNiMnW system demonstrated superior OER kinetics compared with those of its counterparts (Fig. 3(a)). The FCC architecture enables maximized exposure of active metal sites on densely packed (111) crystallographic planes. This under-coordinated environment creates more active sites with unsaturated valence electrons, which are crucial for capturing and activating reactant molecules. Additionally, the HCP arrangement of surface atoms in FCC (111) facets matches the geometric configuration of many reaction intermediates, reducing steric hindrance during the reaction and facilitating the formation of transition states with lower energy barriers. Moreover, the synergistic multicomponent integration of Fe/Co/Ni/Mn/W, coupled with accelerated electron transport facilitated by its symmetrical metallic bonding network and lattice distortion-induced activation achieved through controlled elemental incorporation, collectively enhances the material's performance. Similarly, Chen *et al.* [147] synthesized a $Pt_{34}Fe_5Ni_{20}Cu_{31}Mo_9Ru$ catalyst with an FCC structure for HER. As illustrated in Fig. 3(b), through a controlled reduction process, the initially cubic FCC $Pt_{34}Fe_5Ni_{20}Cu_{31}Mo_9Ru$ nanocrystals underwent facet-selective reconstruction, forming convex cubes characterized by sharp pyramidal protrusions on each surface [148]. This morphological transition is attributed to the anisotropic growth kinetics inherent to FCC systems, where the interplay between metal precursors and reducing agents preferentially stabilizes high-index facets. Moreover, the HER activity order ($Pt_{34}Fe_5Ni_{20}Cu_{31}Mo_9Ru$ > PtFeNiCuMoRu-1 h > PtFeNiCuMo > Pt/C) indicates that the synergistic effect of multiple metal components enhances the catalytic activity for HER (Fig. 3(c)). The close-packed FCC lattice facilitates efficient electron transfer while accommodating multiple alloying elements (Fe, Ni, Cu, Mo, and Ru) through substitutional solid-solution formation. Moreover, He *et al.* [149] noted the precipitation of numerous rhombohedral-structured nanoparticles within the FCC matrix of a FeCoNiMoW HEA. By optimizing and synergistically integrating these five metallic elements, an optimal balance was established in terms of the M–H bond strength and thus the free energy required for hydrogen production. Moreover, the results of characterization combined with theoretical calculations revealed that this remarkable behavior is due to the rhombohedral crystal structure and the self-sustaining "eco-system" enabled by the selective substitution of metal atoms. This structure facilitates efficient electron transfer and significantly lowers energy barriers.

In summary, the effect of the crystal structure is intrinsically linked to composition regulation, as tailoring the elemental composition directly governs the formation and stability of specific crystalline phases. The FCC structure significantly influences the catalytic performance through multiple aspects. Its unique electronic structure, characterized by a symmetrical metallic bonding network, facilitates accelerated electron transport. The surface atom arrangement of the FCC structure, such as the dense packing of (111) crystal planes, maximizes the exposure of active metal sites. Furthermore, the thermodynamic stability of the FCC structure, which is conducive to the formation of a uniform single-phase or ideal solid-solution structure, provides a stable environment for catalytic reactions. These factors collectively contribute to the superior catalytic performance of HEMs with FCC structures.

3.1.2 *Element modulation engineering*

The multi-element composition of HEMs is proposed as a promising platform for catalyst optimization because of its ability to enhance catalytic effects through the influence of synergistic interactions between the various elements on the surface and electronic properties. The inherent electrocatalytic qualities of HEMs are essentially dictated by the controlled elemental composition, and certain specific metal element groups can provide corresponding adsorption/activation sites, thereby resulting in excellent catalytic activity [68,150]. However, the constraint lies in the limited availability of specific metal elements that provide optimal adsorption/activation sites for intermediates, hindering the systematic tuning of catalytic activity in HEMs [151,152]. To overcome this constraint, designing a rational element composition that facilitates the optimal adsorption of crucial intermediates on the catalyst surface and thus maximizes catalytic activity is imperative [87,153]. To achieve these goals, Jia *et al.* [140] synthesized high entropy intermetallic (HEI) materials with an $L1_2$-ordered structure, employing a FeCoNi transition metal combination as the active site and utilizing Al and Ti to refine the ordered atomic configuration. Within this $L1_2$ arrangement, Al and Ti atoms are located at the vertices of the unit cell while the Fe, Co, and Ni atoms are positioned at the face centers, collectively modulating the atomic distribution (Fig. 3(d)). The synergistic chemical interactions and structural site-isolation effects among the various elements within the HEI significantly improve the electrocatalytic performance. The results of density functional theory (DFT) calculations reveal that Ti atoms exhibit a more favorable E_{ad} for H_2O than the other elements, with all the metal sites in the $L1_2$ HEI presenting higher E_{ad} values than those of Pt (Fig. 3(e)). Furthermore, following H_2O adsorption, the results revealed that the single Al coordination site (denoted by weak red shading in Fig. 3(f)) exhibites significant electron depletion, which is attributed to enhancing electron transfer processes during the catalytic reaction.

In PtRuRhCoNi, the interactions among various elements strengthen the coupling between bonding and anti-bonding orbitals, facilitating efficient electron transfer between atomic sites and offering diverse active centers for various electrocatalytic reactions [150]. Such interactions optimize the electronic structure, enabling bifunctional (i.e., oxidation and reduction) activity. In contrast, the bonding and antibonding orbitals on a pure Pt surface are highly ordered (Fig. 3(g)) [150]. This uniformity limits the versatility of Pt as a multifunctional catalyst because of the fixed nature of the active sites. For the PtRuRhCoNi HEM, overlap among the different elements amplifies orbital coupling via a self-complementary effect (Fig. 3(h)), maximizing electron transfer efficiency across sites and allowing for superior catalytic performance.

Shaikh *et al.* [154] synthesized $RuIrFeCoNiO_2$ with abundant grain boundaries (GB), achieving an impressively low overpotential of 189 mV at 10 $mA{\cdot}cm^{-2}$ for the OER under acidic conditions. Their research revealed that incorporating multiple atoms, such as Ir, Fe, Co, and Ni, stabilizes surface oxygen during the OER (Fig. 3(i)). Microstructural analysis and DFT calculations collectively demonstrate that the high-entropy multicomponent strategy is conducive to enhanced activity and stability of RuO_2-based catalysts for the OER [155]. Similarly, Cui *et al.* [69] synthesized $(Cr_2MnFe_2Co_2Ni_2)S_8$ featuring multi-elemental synergistic sites close to the peak of the volcano with nearly neutral adsorption energy, which represents a highly effective choice for the OER. This optimal adsorption energy, a key factor influencing catalytic performance, enables the catalyst to achieve a

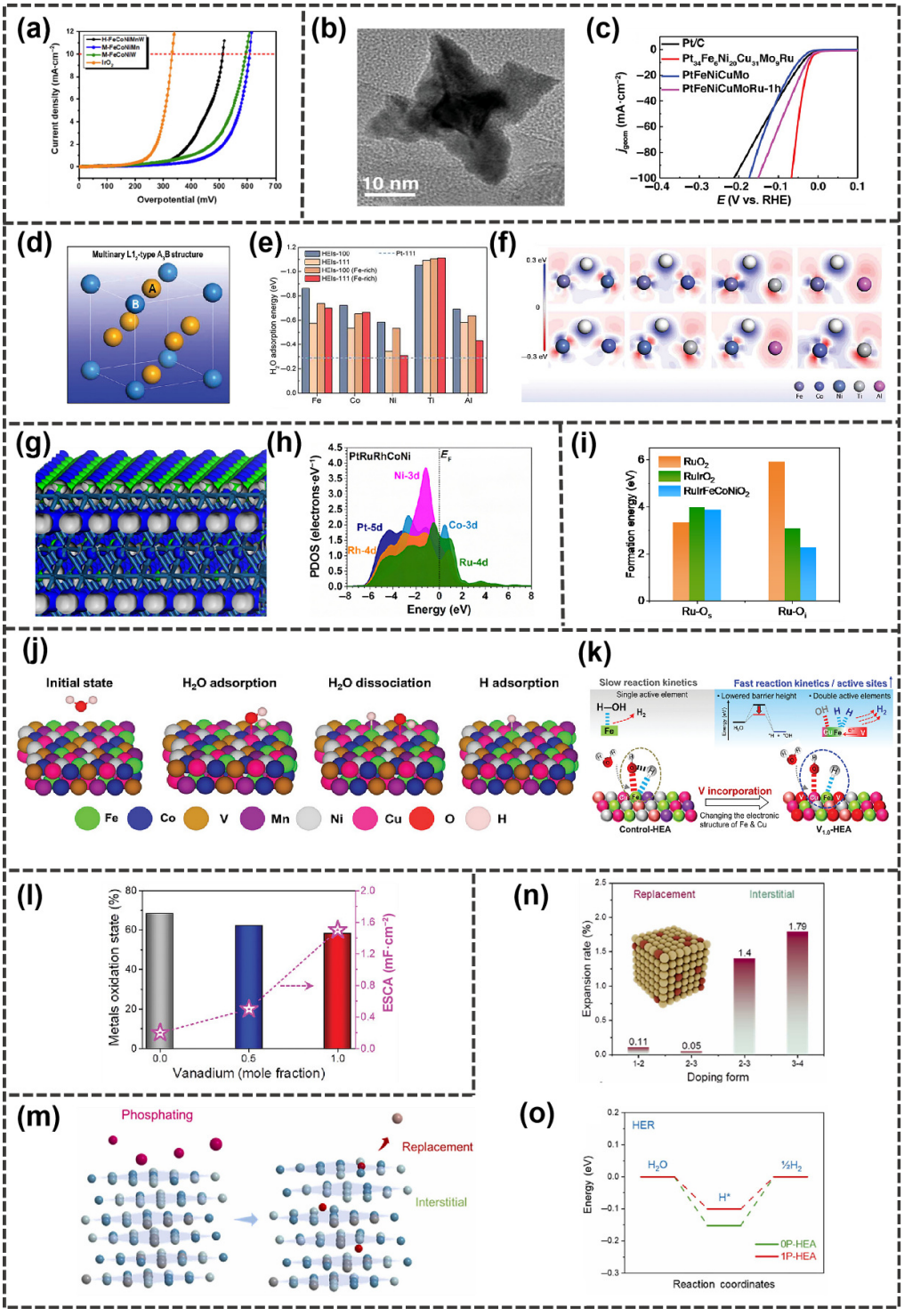

Fig. 3 Effects of crystal structure, element composition, and doping on catalytic activity of HEMs. (a) OER performance of H-FeCoNiMnW, M-FeCoNiMn, and M-FeCoNiW under acidic conditions. Reproduced with permission from Ref. [146], © Elsevier B.V. 2022. (b) TEM image of $Pt_{34}Fe_5Ni_{20}Cu_{31}Mo_9Ru$. (c) Comparison of HER performance for $Pt_{34}Fe_5Ni_{20}Cu_{31}Mo_9Ru$, PtFeNiCuMo, and PtFeNiCuMoRu-1 h. Reproduced with permission from Ref. [147], © Wiley-VCH GmbH 2022. (d) Schematic model of $L1_2$ high-entropy intermetallic (HEI) with A sites occupied by Al and Ti and B sites occupied by Fe, Co, and Ni. (e) E_{ad} of H_2O molecules on various exposed surfaces. (f) 2D electron density differences after H adsorption, where red and blue regions indicate areas of electron depletion and accumulation, respectively. Reproduced with permission from Ref. [140], © WILEY-VCH Verlag GmbH & Co. KGaA, Weinheim 2020. (g) 3D contour plot of electronic distribution near Fermi level for Pt (blue iso-surface corresponds to bonding orbitals, whereas green iso-surface denotes antibonding orbitals). (h) Projected density of states (PDOSs) of PtRuRhCoNi-HEA. Reproduced with permission from Ref. [150], © Elsevier B.V. 2022. (i) Formation energies of surface and subsurface oxygen vacancies (O_s and O_i, respectively) in RuO_2-based catalysts obtained via density functional theory (DFT) calculations. Reproduced with permission from Ref. [151], © 2023 The Authors, some rights reserved; exclusive licensee American Association for the Advancement of Science. (j) An illustration depicting surface atomic arrangement of $V_{1.0}$CuCoNiFeMn with adsorbed and dissociated H_2O and adsorbed H. (k) Proposed effect of incorporating V on HER mechanism on a V_xCuCoNiFeMn electrode. (l) Correlation between metal oxidation state, electrochemical surface area (ECSA), and V content in V_xCuCoNiFeMn. Reproduced with permission from Ref. [152], © Wiley-VCH GmbH 2023. (m) Model of P doping in $Ni_{30}Co_{30}Fe_{10}Cr_{10}Al_{18}W_2$ HEA. (n) Calculated lattice expansion rates resulting from P doping. (o) Changes in Gibbs energy during HER for undoped (0P-HEA) and P-doped (1P-HEA) $Ni_{30}Co_{30}Fe_{10}Cr_{10}Al_{18}W_2$. Reproduced with permission from Ref. [131], © Elsevier Ltd. 2023.

balance between reactant binding and product release. The synergistic regulation of multi-element interactions in high-entropy metal sulfides leads to a change in the surface charge of the catalyst and hence the binding of adsorbents, significantly enhancing the OER activity of $(Cr_2MnFe_2Co_2Ni_2)S_8$ nanoparticles. In addition, Yang *et al.* [156] reported chemical short-range order (CSRO) in $Fe_{10}Co_5Ni_{10}Cu_{15}Al_{60}$, which was driven by the magnetic properties of the constituent elements. This non-random atomic arrangement resulted in an exceptionally low overpotential for dual-functional water splitting under alkaline conditions. Transmission electron microscopy (TEM) imaging and DFT calculations demonstrated that the CSRO originated from the preferential pairing of M–Cu (M = Fe, Co, Ni, or Al) and the repulsion between identical atomic pairs (Fe–Fe, Co–Co, Ni–Ni, Cu–Cu, or Al–Al). These tailored atomic configurations optimize H* adsorption and desorption during the HER and reduce the energy barrier for the RDS in the OER, leading to a remarkable overall water-splitting performance.

In conclusion, synergy among elements is crucial for optimizing the performance of HEMs during catalytic reactions. The unique combination of elements promotes the formation of diverse active sites, which synergistically increase the density and activity of the reactive centers. This enhanced catalytic activity can be attributed to the tailored electronic environments and surface structures enabled by the multielement composition.

3.1.3 *Metal element modification*

The catalytic performance of HEMs can be further optimized by strategically tailoring the electronic structure through doping with new elements. Heteroatom doping stands out as a particularly effective strategy to modulate the electronic configuration and catalytic behavior of host materials by promoting charge redistribution [123,157,158]. In particular, by introducing heteroatoms with varying electronegativities, the charge redistribution can significantly improve the electrochemical activity of a catalyst without altering the fundamental composition of the host materials [159–161]. Recent studies have demonstrated that doping appropriate elements can also finely tune the lattice parameters and interatomic interactions of catalysts, which can lower the reaction activation energy and facilitate charge transport by introducing lattice distortions and altering the local electronic structure [162,163]. Metal element doping, involving elements such as Co, Ni, Na, Zn, La, and V, has been shown to markedly enhance the electrochemical properties of HEMs. Specifically, the introduction of metal elements can optimize the charge distribution, regulate the electronic structure, and increase the number of active sites of HEMs. This can optimize ion conduction pathways and enhance the electronic conductivity, thereby improving the electrochemical performance [164].

Sivanantham *et al.* [152] explored the impact of V incorporation on the physicochemical characteristics and electrochemical performance of CuCoNiFeMn with an FCC structure. The addition of V significantly reduced the Gibbs energy associated with both water dissociation and hydrogen adsorption (Fig. 3(j)), thereby accelerating hydrogen adsorption (H*) and H_2 formation for efficient water splitting. Importantly, V incorporation modifies the electronic configuration of neighboring elements, especially Cu and Fe, through electron sharing with high-valence V. This mechanism facilitates water adsorption and dissociation on adjacent Fe sites, lowering the binding energy barrier via efficient electron transfer (Fig. 3(k)). Additionally, the incorporation of V alteres the preoxidation state of Co, Ni, Fe, and Mn (Fig. 3(l)), accompanied by significant changes in the surface elemental composition. These alterations reduce the binding energy barrier of intermediates and increase the charge transfer efficiency during the water splitting process.

3.1.4 *Anion modification*

Numerous studies have demonstrated that anion modifications lead to better adsorption properties than metal cation modifications for specific reaction intermediates. While metal atoms are often considered the primary active sites, the surrounding anions play a role in controlling the electronic structure of the metal atoms and hence the inherent catalytic activity [58,165,166]. Li *et al.* [58] introduced an innovative class of high-entropy electrocatalysts based on non-noble metals, achieved by incorporating a P-modified CoFeNiCrMn alloy on nickel foam (NF). The strategic synergy between the P anions and the five metal elements significantly accelerated the reaction kinetics, particularly for the HER. For the HER, the CoFeNiCrMnP/NF catalyst demonstrated remarkable performance with a low overpotential of 51 mV at 100 $mA{\cdot}cm^{-2}$, a small Tafel slope of 48 $mV{\cdot}dec^{-1}$, and excellent stability under alkaline conditions. Previous studies have indicated that the incorporation of P anions tunes the electronic structure and optimizes the adsorption free energy of reaction intermediates on the catalyst surface, which in turn significantly enhances the catalytic activity [167–169].

Chen *et al.* [131] reported that incorporating P atoms into a $Ni_{30}Co_{30}Fe_{10}Cr_{10}Al_{18}W_2$ HEA could introduce lattice strains, effectively tailor the intrinsic electronic structure, and significantly enhance the catalytic performance (Fig. 3(m)). The larger atomic radius of the P atom, in comparison with the octahedral interstice in the FCC lattice, causes a substantial expansion of the lattice when P occupies interstitial sites. In contrast, substitutional P atoms cause only a relatively modest expansion (Fig. 3(n)). This disparity gives rise to a nonuniform distribution of lattice strain throughout the depth profile. As depicted in Fig. 3(o), the HER Gibbs energy profiles for the P-doped and undoped systems reveal that the P-doped $Ni_{30}Co_{30}Fe_{10}Cr_{10}Al_{18}W_2$ demonstrates a reduced Gibbs energy change for the rate-limiting step ($H^* \rightarrow \frac{1}{2}H_2$) compared with that of the undoped HEA. Therefore, the optimized P-HEA electrode, featuring the highest dopant concentration (2.88 at%) and maximum lattice strain (1.13%), exhibits remarkably low overpotentials of 70 and 211 mV at 10 $mA{\cdot}cm^{-2}$ for the HER and OER, respectively. The significant improvement in HER efficiency is predominantly ascribed to electronic coupling between the P atoms and the HEA surface. Specifically, electrons from the P atoms partially occupy the bonding orbitals on the surface and establish a strong π interaction with the d orbitals of the metal atoms. This interaction attenuates the σ bonding strength between hydrogen and the metal, facilitating more efficient hydrogen desorption.

In addition to P doping, the introduction of orbital contributions from other nonmetallic elements (e.g., N, P, S, Se, and Te) into HEMs has been shown to significantly increase catalytic activity by inducing new phases or modifying existing phases [170–172]. This improvement stems from the versatile chemical design offered by multi-component systems. In a notable study, Jo *et al.* [173] strategically employed Co, Fe, and Ni as catalytically active 3d transition metals, Mo and W as passivating metals, and Te as a nonmetallic component to engineer OER electrocatalysts with an optimal balance between activity and durability. Compared with amorphous CoFeNiMoW, the incorporation of Te into CoFeNiMoW nanosheets results in the formation of crystalline structures with more diverse electronic states. Among the chalcogen elements, Te stands out because of its exceptionally rich electronic states and diverse coordination

numbers, both of which are crucial for enhancing the catalytic performance. Jo *et al.*'s study [173] has revealed that amorphous nanosheet arrays of CoFeNiMoWTe as electrocatalysts exhibit a higher density of active sites and promote elevated metal valence states, in contrast to the spherical-shaped CoFeNiMoW electrocatalysts lacking Te. These phase changes directly impact the active site density and metal valence state, thereby increasing the catalytic activity.

In summary, the doping strategy can further increase the adsorption capacity and intermediate activation of catalysts by tuning the electron density and lowering the energy barriers, thereby resulting in a marked increase in catalytic performance. Furthermore, the introduction of foreign elements into HEMs promotes substantial variation in the electronic properties of the surface metal atoms. This facilitates an enhanced redistribution of charge atoms and hence adsorbed molecules, offering improved catalytic activity. Metal element doping mainly alters the host material's electron density, optimizing the adsorption/desorption free energy of reaction intermediates (e.g., *OH, *O, and *OOH for the OER; *H for the HER), whereas anion doping works by adjusting the surrounding environment or forming a new active site. Anion doping can also stabilize the valence state of the hypervalent metal, reducing the activation energy of reactions to form a more stable intermediate product and thereby increasing the reaction kinetics.

3.2 Strain engineering

Compared to heteroatom modification, strain engineering emphasizes tuning the intrinsic physiochemical properties of HEMs rather than introducing foreign elements [174,175]. Strain engineering serves as a pivotal strategy for modulating the interactions between catalytic surfaces and adsorbate molecules, achieved by modifying the electronic and geometric structures of the metal active sites. This approach provides an effective mechanism for tailoring the electronic structures of HEM-based catalysts [85,176]. The substantial intrinsic lattice strain in HEMs endows them with elevated potential energy, surpassing that of their binary or ternary counterparts [85]. This unique feature results in reduced energy barriers during HEM-catalyzed reactions, facilitating the desired chemical transformations [177]. The core principle of strain engineering lies in strategically inducing compressive or tensile atomic arrangements, which induce the shifts in the d-orbital density centers relative to the Fermi level [176]. Moreover, in HEMs, the interplay among the d-bands of constituent metal elements modulates the d-band centers of the active sites, effectively tuning the binding energy of critical intermediates and significantly improving the catalytic efficiency toward the intended product [80]. The distinct electronic modifications in HEMs suggest the presence of "hidden" factors that determine the relationships between catalytic functionalities and the structures and properties of materials.

Catalytic activity is predominantly dictated by the intrinsic electronic structure of a material. Hence, d-band theory has emerged and has been progressively refined to provide insights into this phenomenon. The d-band center (ε_d) denotes the average energy level of the d-orbitals relative to the Fermi level (E_f), offering a predictive framework for the adsorption energies of reactants and intermediates on a catalyst surface [101]. It serves as a critical descriptor for adsorption energetics in catalysis. Central to this theory is the principle that the d-band center location governs the interaction strength between adsorbates and the catalyst surface, thereby shaping its catalytic performance. A higher ε_d typically strengthens adsorbate binding, while a lower ε_d weakens it [178,179]. In the context of electrocatalysts, surface strain alters the interatomic spacing and electronic structure, thereby shifting the d-band center. Strategic modulation of the d-band center and hence the reaction barriers on the catalyst surface can be achieved by manipulating the surface strain and enabling fine-tuning of the electrocatalytic properties [180].

Kwon *et al.* [130] studied the impact of d-band center shifts in ZnNiCoIrX (X = Fe, Mn) (Fig. 4(a)) by examining alterations in the Ir electronic structure resulting from the incorporation of Mn atoms. As the number of metal elements increases, electron transfer from 3d transition metals to Ir significantly alters the electron density distribution around Ir within ZnNiCoIrX. The incorporation of Mn results in a pronounced shift in the Ir 4f peak in the XPS spectra, surpassing that observed with Fe incorporation in ZnNiCoIrMn, indicating pronounced electron redistribution. Additionally, the incorporation of Mn shifts the d-band center of ZnNiCoIrMn to a more negative value (Fig. 4(b)), resulting in weaker hydrogen bonding than that of ZnNiCoIr. This facilitates the desorption of hydrogen, thereby enhancing the HER activity (Fig. 4(c)).

Similarly, the results reported by Wang *et al.* [128] also demonstrated that a substantial improvement in HER electrocatalytic performance is intricately linked to a downward shift in the d-band center. As shown in Figs. 4(d) and 4(e), highly ordered $Pt_4FeCoCuNi$ has a d-band center that is closest to the Fermi level, which leads to weaker adsorption energies for HER intermediates than those of their more disordered counterparts. Consequently, highly ordered $Pt_4FeCoCuNi$ displays superior HER activity compared with commercial Pt/C and more disordered $Pt_4FeCoCuNi$, achieving an overpotential of 20 mV at 10 $mA{\cdot}cm^{-2}$ (Fig. 4(f)).

Hu *et al.* [181] reported the *in situ* reconstruction of non-noble HEA–HEO FeCoNiMnCr heterostructures, achieving remarkable stability for the OER. The HEA–HEO catalyst was fabricated by an *in situ* phase transition process of the HEA triggered by early transition metals, which generates abundant HEA–HEO interfaces. These heterostructures improve the stability of metal particles during the OER process by leveraging the robust interactions between the alloy and the oxide components. For the HEA, strong d–d coupling arises from overlapping 3d orbitals of the various metals (Fig. 4(g)). However, the transition to HEO induces a reduced overlap of the 3d orbitals (Fig. 4(h)). Notably, the upward shifts of the Ni 3d and Co 3d orbitals, relative to their positions in the HEA, correspond to an increase in electroactivity. Concurrently, the peaks of the Fe 3d and Mn 3d orbitals narrow, whereas the Cr 3d orbitals exhibit a relative shift with respect to Mn 3d. These orbital adjustments not only increase the electron density near E_f but also preserve the stability of the Ni and Co valence states, thereby contributing to durable OER performance. Furthermore, it has been proposed that the repulsive interactions between oxide species in HEO and oxygen-containing intermediates weaken their binding to adjacent active metal sites, accelerating OER kinetics [181].

Thus, the d-band centers of the metals in electrocatalysts play a critical role because orbital hybridization between the adsorbate and the metal center governs the adsorption/desorption behavior. However, the manipulation of 3d electron energies in transition metals in HEMs has received limited research attention because of the inherent challenges in precisely controlling their coordination environments. Further research is essential to unravel the unique electronic structure of HEMs.

3.3 Electronegativity difference

A substantial electronegativity difference between atoms can reduce the miscibility of constituent elements in a HEM, thereby

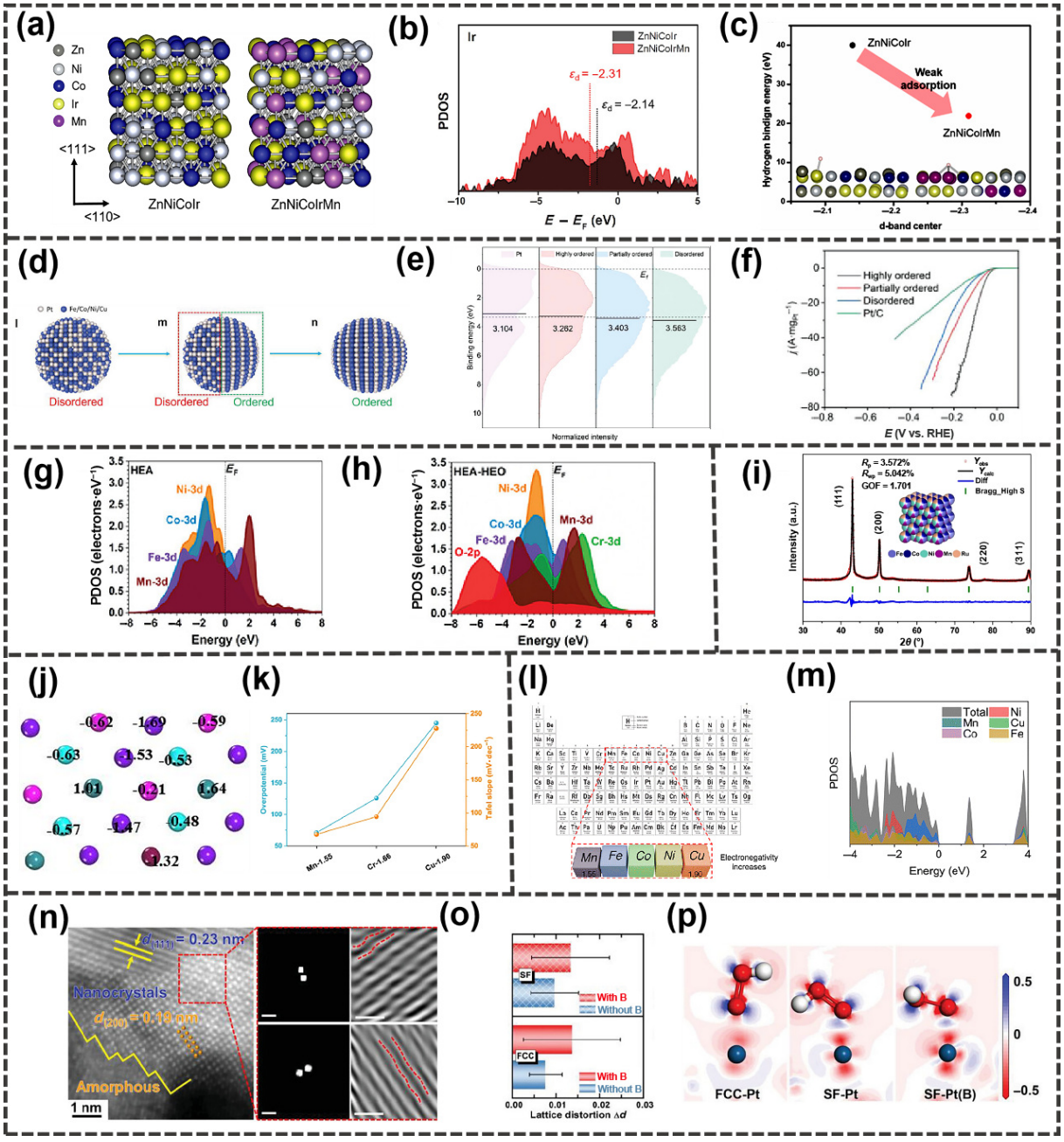

Fig. 4 Effects of d-band center shift, electronegativity differences, and defects on catalytic performance of HEMs. (a) Computational models of ZnNiCoIr and ZnNiCoIrMn. (b) Projected d-band partial density of states for Ir in both ZnNiCoIr and ZnNiCoIrMn. (c) Correlation between d-band center and hydrogen binding energy. Reproduced with permission from Ref. [130], © Wiley-VCH GmbH 2023. (d) Schematic representation illustrating alteration in atomic arrangements of $Pt_4FeCoCuNi$ between ordered and disordered samples. (e) XPS valence band spectra for highly ordered, partially ordered, and disordered $Pt_4FeCoCuNi$ catalysts and Pt foil. (f) Linear sweep voltammetry curves for $Pt_4FeCoCuNi$ and Pt/C showing a difference in overpotentials. Reproduced with permission from Ref. [128], © Wiley-VCH GmbH 2023. PDOS of (g) FeCoNiMnCr HEA and (h) HEA–HEO. Reproduced with permission from Ref. [181], © Wiley-VCH GmbH 2024. (i) XRD patterns of FeCoNiMnRu/CNFs. (j) Bader charge analysis of FeCoNiMnRu system. (k) Relationship between OER overpotential and electronegativity of metal X in FeCoNiXRu (X = Cr, Mn, or Cu). Reproduced with permission from Ref. [108], © The Author(s) 2022. (l) Electronegativity rankings for Mn, Fe, Co, Ni, and Cu. (m) PDOS for d orbitals of Fe, Co, Ni, Cu, and Mn, along with total DOS for FeCoNiCuMn. Reproduced with permission from Ref. [182], © Royal Society of Chemistry 2023. (n) HAADF-STEM image with lattice distortion, (o) extent of lattice distortion (Δd) in FCC and SF structures for $(FeCoNiB_{0.75})_{97}Pt_3$ HEMG, both in presence and absence of B, and (p) 2D electron density differences following OOH* adsorption on different Pt active sites. Reproduced with permission from Ref. [132], ©Wiley-VCH GmbH 2023.

affecting phase stability or encouraging phase separation [177,183,184]. In a pioneering investigation, researchers explored how the electronegativity disparities among multiple metals in HEMs affect the competitive adsorption of intermediates involved in the alkaline HER and OER. Hao *et al.* [108] studied the charge transfer dynamics among the surface atoms in FeCoNiMnRu HEAs, which are composed of five principal elements with various electronegativities, synthesized on carbon nanofibers (CNFs). The supporting evidence from the X-ray diffraction (XRD) analysis confirmed the development of a single-phase HEA structure in the FeCoNiMnRu NPs (Fig. 4(i)). Relative to the standard diffraction patterns of the FeNi alloy (PDF#47-1417), the diffraction peaks corresponding to the FCC phase of the FeCoNiMnRu HEAs were slightly shifted to lower angles, which

was attributed to lattice distortions induced by the introduction of the Ru, Mn, and Co atoms. In the FeCoNiMnRu HEA, the varying electronegativity values of Fe(1.83), Co(1.88), Ni(1.91), Mn(1.55), and Ru(2.20) drive substantial charge redistribution (Fig. 4(j)). This redistribution results in the activation of Co and Ru sites, which feature optimized energy barriers that efficiently stabilize OH* and H* intermediates, thereby significantly enhancing the catalytic efficiency. Considering the OER activity of FeCoNiXRu/CNFs (X = Mn, Cr, and Cu) (Fig. 4(k)), the comparatively low electronegativity of Mn (1.55), compared with that of Cr (1.66) and Cu (1.90), facilitates exceptional OER performance, as evidenced by the minimal overpotential at 100 $mA{\cdot}cm^{-2}$.

Building upon these insights, Zhu *et al.* [182] presented an innovative strategy for regulating the electrocatalytic behavior of FeCoNiCuMn HEA NPs by leveraging an electronegativity-driven approach to optimize competitive adsorption sites. By incorporating Fe, Co, and Ni as primary components, alongside low-electronegativity Mn and high-electronegativity Cu, a single-phase FCC HEA was successfully synthesized via a polymer fiber nanoreactor method (Fig. 4(l)). Both experimental data and theoretical analyses reveal that significant local electron interactions, driven by variations in electronegativity among the constituent metal atoms, result in an increase in electron density at the Ni and Cu sites while simultaneously depleting it at the Mn, Co, and Fe sites (Fig. 4(m)). This electronegativity-driven redistribution of local electrons converts inert Cu into electron-rich active sites for the HER and OER, effectively lowering the adsorption energies of the reactants, intermediates, and products and significantly increasing the electrocatalytic performance. Leveraging its competitive preferential adsorption capabilities, the HEA demonstrates exceptional catalytic efficiency for both the HER and OER, coupled with remarkable cycling stability.

3.4 Defect engineering

To optimize the catalytic activity of multi-element systems, introducing defects to create synergy with the multiple metals present has proven to be effective. Defect engineering has emerged as a compelling approach to enhancing electrochemical reactivity by tuning the electronic structure of materials [164]. Structural defects, including dislocations, vacancies, and grain boundaries, serve as catalytically active sites by modifying the adsorption characteristics of reactants and providing alternative reaction mechanisms [139,185,186]. Zhang *et al.* [132] engineered a nanoporous, defect-enriched nanocrystalline surface in a high-entropy metallic glass (HEMG) of $(FeCoNiB_{0.75})_{97}Pt_3$. The partial dealloying process led to the formation of nanocrystals distributed along the nanopores, with the resulting materials characterized by pronounced lattice distortion (LD) and a high density of stacking faults (SFs) due to the incorporation of interstitial B atoms. This distinctive architecture not only maximizes the specific surface area but also offers an abundance of active sites, significantly enhancing the water electrolysis efficiency (Fig. 4(n)). Notably, the insertion of B into the FCC and SF regions substantially increased the degree of LD (Δd) (Fig. 4(o)), indicating that the increased LD observed in the nanocrystals originates from the formation of an interstitial solid solution of B. DFT calculations revealed that the Fe and Co sites in the SF structure presented the highest H_2O adsorption energies (ΔE_{H_2O}) of −0.70 and −0.44 eV, respectively, significantly exceeding the benchmark value for Pt (111). Notably, Pt and Ni sites with B coordination display higher ΔE_{H_2O} values than those without B coordination, indicating that the LD induced by interstitial B atoms is a contributing factor to the increase in ΔE_{H_2O}. These structural defects also influence the OER activity. A comparative analysis of the ΔG values at the active sites of SF–Pt and SF–Pt(B) indicates that the RDS ($\Delta G_3 = \Delta G_{OOH^*} - \Delta G_{O^*}$) for the SF–Pt(B) site results in a lower ΔG_3 value of 1.84 eV than the value of 1.92 eV for SF–Pt. These findings highlight the enhanced electron-transfer capability of the SF–Pt(B) site toward the OOH*intermediate in the OER (Fig. 4(p)).

The introduction of oxygen vacancies (O_{Vs}) has also emerged as a key strategy for enhancing electrocatalysis in HEMs. Liao *et al.* [77] highlighted the crucial role of O_{Vs} in regulating the catalytic performance of HEMs. They synthesized HEOs with up to 35.3% O_{Vs} via resin templating and precise thermal treatment, forming nanosphere-like structures with stable crystallinity. O_{Vs} was characterized by EPR (characteristic signal at g = 2.002) and XPS (O 1s spectra fitting to quantify vacancy oxygen), confirming their high abundance. Mechanistically, high-degree O_{Vs} modulate metal activation states, enhancing both HER and OER activities by optimizing electronic structures and increasing the number of active sites. The presence of O_{Vs}, along with the key roles of Fe and Cr, enables efficient overall water splitting, underscoring the importance of O_{Vs} in tuning the catalytic properties of HEMs. High-oxygen vacancies (35.3%) in high-entropy oxides enhance HER and OER activity by modulating the metal states and electronic structure, enabling efficient water splitting.

Overall, defects are not only prevalent but also often inevitable in fabricated electrocatalytic materials. During the process of water electrolysis, these defects serve as active sites and nucleation centers, facilitating the construction of highly active components. Surface defect sites can effectively capture and anchor metal species, ensuring the uniform distribution and stability of metal sites in electrocatalysts. Specifically, the introduction of defects significantly modulates the local electronic structure, promotes synergistic interactions, and generates additional active sites.

3.5 Morphology regulation

3.5.1 *Morphology effect*

In addition to the factors discussed above, the morphological structure can significantly influence the catalytic performance [85,187]. The focus of morphological regulation typically lies in two key aspects: reducing the particle size and increasing the specific surface area [120,188,189]. Previous studies have shown that microscale porous materials, characterized by large surface areas and tunable structures, are pivotal in enhancing the electron transport process during electrocatalysis, as more active sites are exposed on the surface area [136,165]. Recently, Huang *et al.* [137] devised a FeCoNiRu electrocatalyst synthesized from high-entropy metal–organic framework (HEMOF) precursors. The substantial porosity and accessible surface area of the MOFs minimize the required diffusion distances for charge carriers during electrocatalysis [190]. As depicted in Figs. 5(a) and 5(b), FeCoNiRu-450 nanoparticles (heat treated at 450 °C during synthesis) are uniformly distributed across the carbon skeleton. The porous carbon framework derived from the MOF precursor not only facilitates the rapid transport of reaction species but also inhibits excessive nanoparticle growth [137]. Under an applied external potential or current, the hollow active sites within the spinel structure, which maintain the initial characteristics, further contribute to this enhanced performance (Fig. 5(c)). Thus, employing morphology structural engineering of HEMs at mesoscopic and microspatial scales effectively enhances their electrochemical surface areas, improves their ion and electron transport kinetics, and ultimately increases their charge transfer efficiency in electrocatalytic applications [164,191].

Wang *et al.* [192] developed $FeCoNiCuAl_2Mn$ materials

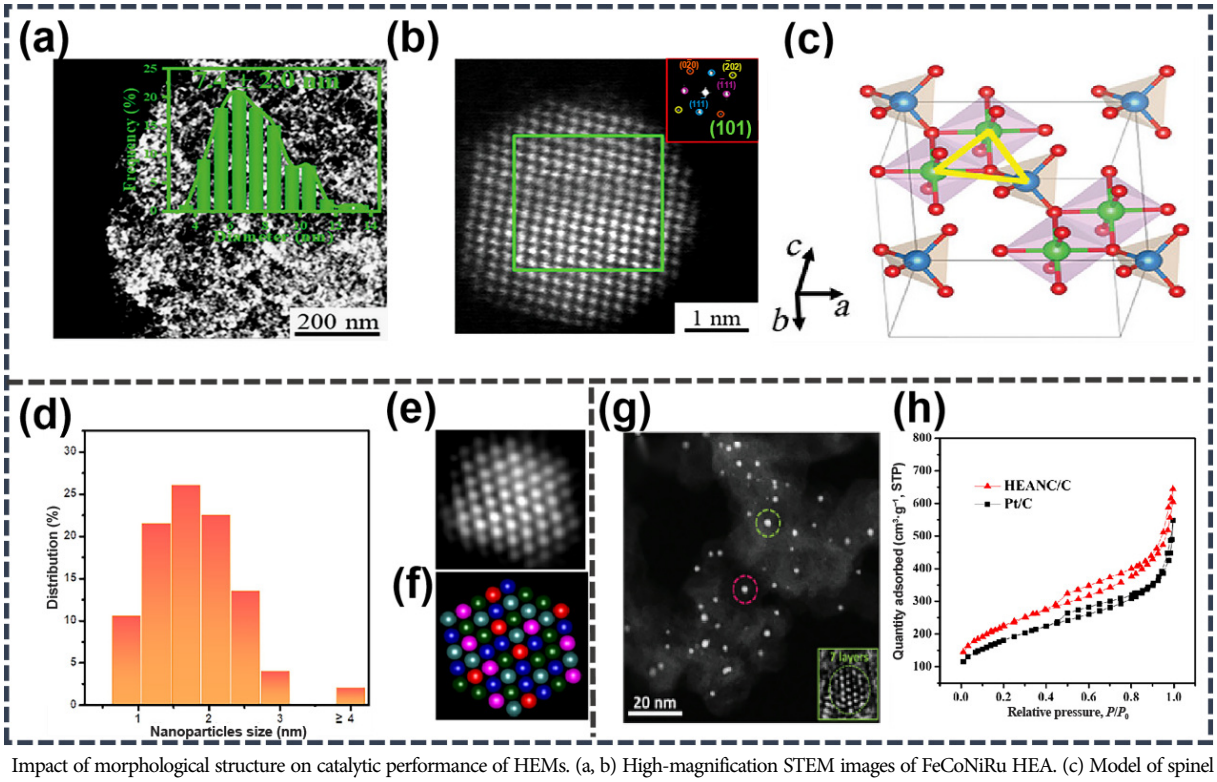

Fig. 5 Impact of morphological structure on catalytic performance of HEMs. (a, b) High-magnification STEM images of FeCoNiRu HEA. (c) Model of spinel oxide. Yellow triangle indicates hollow site of FeCoNiRu-450. Reproduced with permission from Ref. [137], © The Authors 2023. (d) Size distribution histogram, (e) Fourier-filtered image, and (f) simulated crystal structure representation of NiCoFePtRh us-HEA NPs. Reproduced with permission from Ref. [195], © American Chemical Society 2021. (g) HAADF-STEM image of NiCoMoPtRu HEANCs. (h) Nitrogen adsorption–desorption isotherms for HEANC/C and Pt/C catalysts. Reproduced with permission from Ref. [196], © Wiley-VCH GmbH 2023.

featuring a hierarchical porous sandwich-like configuration. This architecture enhances surface hydrophilicity and mass transfer efficiency during electrocatalysis [176,193]. The hydrophilicity was evaluated via water contact angle measurements, which revealed a significant reduction from 84.4° to 63.1°, 57.7°, 39.2°, 25.4°, and 25.7° after 100, 200, 300, 400, and 500 h of dealloying, respectively. The $FeCoNiCuAl_2Mn$-400 sample exhibited exceptional hydrophilicity. This innovative design significantly improves surface hydrophilicity and facilitates efficient mass transfer during electrocatalytic processes. Cui *et al.* [194] also presented a core–shell FeCoNiMoAl HEA as a promising OER electrocatalyst. DFT calculations revealed that the crystalline–amorphous (c–a) heterostructure of the shell reduces the electron transfer resistance, whereas the crystalline core enhances the conductivity and self-supporting ability. Notably, the crystalline–amorphous interface in the shell facilitates charge redistribution, optimizes the adsorption energies of oxygen intermediates, and provides abundant active sites. The HEA electrodes exhibited superior OER performance, with an overpotential of 470 mV at 2 $A{\cdot}cm^{-2}$ and excellent stability for 330 h. This core–shell strategy design represents a promising strategy for developing efficient and durable electrocatalysts for industrial water electrolysis.

3.5.2 *Nanosizing effect*

Decreasing the particle size has been extensively investigated as a strategy to expose more active sites and increase both the specific surface area and surface free energy, thereby lowering the catalytic reaction barriers and improving catalyst utilization in reactions [197,198]. The central challenge lies in precisely controlling the nanoscale dimensions of active materials and ensuring the optimal distribution of nanoparticles within composites [199]. Unlike conventional bulk alloys, Feng *et al.* [195] demonstrated that ultrasmall NiCoFePtRh high-entropy alloy particles (us-HEA) loaded on carbon supports exhibit significantly enhanced HER activity (Fig. 5(d)). Fourier-filtered and simulated crystal structure images (Fig. 5(e) and 5(f)) show that the us-HEA NPs have an edge length of merely 4–5 atoms, underscoring their ultrasmall scale. This nanostructure notably enhances the efficiency of utilizing noble Pt atoms. Moreover, the altered electronic structure of Pt in the us-HEA results in an optimized Pt–H binding value, facilitating rapid H^+ adsorption and H_2 desorption and ultimately accelerating HER performance. The same group also synthesized ultrasmall NiCoMoPtRu alloy nanoclusters (HEANCs) (Fig. 5(g)), which require an exceptionally low overpotential of merely 9.5 mV at 10 $mA{\cdot}cm^{-2}$ for the alkaline HER [195]. An investigation of the origins of such superior catalytic activity, using the Brunauer–Emmett–Teller (BET) technique combined with the electrochemical double-layer capacitance (C_{dl}) method, unequivocally demonstrated that HEANCs exhibit an exceptionally high active surface area along with remarkable atom utilization efficiency (Fig. 5(h)), both of which contribute to their outstanding performance in the HER. Similarly, Hu *et al.* [200] also confirmed that ultrasmall PtRhNiFeCu HEA nanoparticle catalysts exhibit outstanding catalytic efficiency for the HER. For the alkaline HER, PtRhNiFeCu/C achieves an impressively low overpotential of just 13 mV at −10 $mA{\cdot}cm^{-2}$ and an exceptionally low Tafel slope of 29.8 $mV{\cdot}dec^{-1}$, both of which surpass those of PtRhNi/C and Pt/C. These findings underscore the necessity of reducing the particle size through appropriate modification techniques to maximize the catalytic performance. In addition, Chang *et al.* [91] synthesized ultrasmall $(FeCoNiRuMn)_3O_{4-x}$ NPs supported on a carbon substrate, which exhibited remarkable electrocatalytic performance characterized by a low overpotential of 230 mV at 10 $mA{\cdot}cm^{-2}$ for the OER, along with remarkable long-term stability over 100 h. The nanosizing effect can not only increase the availability of active sites but also accelerate the

reaction kinetics in HEMs, making it a pivotal approach for advancing HER catalysis.

Overall, the microstructure and morphology of materials significantly affect their electrocatalytic performance. Generally, porous structures are more conducive to catalytic reactions. This design not only enhances the permeation and diffusion of electrolytes into the electrocatalyst, ensuring optimal contact between reactants and active sites within the materials, but also provides additional and shortened pathways for charge transport during water splitting. Furthermore, the development of small particles often increases the density of active sites on HEMs. From a kinetic perspective, minimizing the particle size significantly expands the specific surface area, providing a greater abundance of reactive sites for the HER and OER. Within a certain small size range, a decrease in material size markedly increases atomic exposure, which can lead to notable alterations in the electronic structure. Exploiting the small-sized morphology and the potential synergies of multiple components can lead to enhanced catalytic properties.

3.6 Interaction between HEMs and supports

In electrocatalysis, high conductivity is essential. However, the interaction between HEMs and their supports extends significantly beyond this [201]. Crucially, a robust interface enhances catalyst stability by strongly anchoring nanoparticles, preventing detachment, migration, and agglomeration under dynamic conditions [162,202]. More importantly, this interface facilitates electronic modulation. The intimate contact enables charge transfer between the HEM nanocrystals and the support, potentially altering the electronic structure of HEM and optimizing the adsorption/desorption behavior of key intermediates at the active sites [203]. This synergistic interaction not only ensures long-term durability but also actively contributes to improving the intrinsic catalytic activity [162,204].

3.6.1 *Carbon substrate loading*

In nanoparticle catalysis, supports serve a dual function. They not only enhance stability through charge transfer but also serve as promoters or even take on roles as catalytically active components [205]. For optimal interaction with HEMs, support materials should possess surface chemistries that are compatible, a well-defined pore architecture, and high thermal stability. Carbon-based materials are the most widely utilized supports in electrochemical reactions owing to their outstanding electrical conductivity and widespread availability. Wang *et al.* [23] developed an FeCoNiAlMo alloy integrated with carbon nanotubes (CNTs) as the supporting framework. In the FeCoNiAlMo/CNT composite, the CNTs serve not only as inert carriers but also as active contributors to the system's functionality. The CNTs effectively prevent aggregation of HEA nanoparticles during synthesis, ensuring uniform distribution and stabilization of the quinary FeCoNiAlMo nanoparticles on their surface. Moreover, electronic interactions between the HEA and CNT support modulate the surface chemical states of the HEM. X-ray photoelectron spectroscopy (XPS) analysis revealed that Al and Mo in the FeCoNi lattice, combined with the CNT support, redistributed local charges and increased the ratios of oxidized Co, Ni, and Fe species. This electronic modulation strengthens the adsorption of reaction intermediates, as supported by DFT calculations showing more negative adsorption energies. Consequently, FeCoNiAlMo/CNT exhibited remarkable OER performance, characterized by a low overpotential of 311 mV at 100 $mA{\cdot}cm^{-2}$ and a Tafel slope of 42.9 $mV{\cdot}dec^{-1}$. These outstanding metrics can be ascribed to the synergistic effects of reduced charge transfer resistance and accelerated reaction kinetics.

3.6.2 *Functional group-modified carbon carrier loading*

Carbon substrates can be tailored by incorporating functional groups such as NH_x or N, imparting positive charges that enhance the dispersion of catalysts on the carbon framework [206–208]. For example, functionalizing CNTs with pyridine or hydroxyproline groups establishes robust π–π interactions, thereby improving both electron transfer efficiency and operational stability [118,209]. Recently, Wang *et al.* [210] successfully synthesized PdPtRhIrRu HEA nanocrystals supported on N-enriched graphene (HEA/HNG), which are rich in M-pyridinic N–C bonds (Fig. 6(a)). This configuration facilitates the generation of a directed electron flux at the metal–carbon interface, driven by the disparity in Fermi energy levels between the metal nanoparticles and the N-doped carbon substrate. Notably, the increase in pyridinic N content further intensifies charge redistribution at the interface (Figs. 6(b) and 6(c)). These findings provide strong evidence of significant electronic interactions between N-enriched graphene and HEA nanocrystals. Furthermore, the surface Bader charge distributions of the HEA on N-doped graphene (Fig. 6(d)) were calculated and analyzed. A higher density of M-pyridinic N–C bonds significantly facilitates surface charge redistribution within the HEA, intensifying the electron-deficient state of the nanocrystals. This intensified electron deficiency promotes more efficient H_2O adsorption at the Pd/Ru/Rh sites, whereas the Ru/Ir/Rh sites exhibit a remarkably low energy barrier for H_2O dissociation [210].

There is no doubt that the electronic conductivity of materials is a crucial determinant of high electrocatalytic efficiency in water splitting. While HEMs inherently demonstrate considerable activity even without a substrate, their catalytic performance can be markedly improved by dispersing them on a suitable support. Broadening the range of available conductive substrates for HEMs is essential for unlocking diverse catalytic pathways in water-splitting reactions, encompassing both HER and OER processes.

3.7 Prediction and analysis of element combinations

To scale up water electrolysis via HEM catalysts, identifying electrocatalysts with exceptional efficiency is essential. While the intrinsic compositional complexity of HEMs presents remarkable opportunities for the advancement of high-performance catalysts, it simultaneously poses considerable challenges in pinpointing optimal compositions via traditional trial-and-error approaches. Given the impracticality of exhaustive manual screening, developing a strong foundational understanding of the mechanisms and intricate relationships among composition, structure, and activity to guide rational selection is vital for identifying the most promising compositions for HEM catalysts. Theoretical calculations are indispensable for helping achieve this goal and for uncovering the catalytic mechanisms and their relationships with electronic structures [164]. Thus, integrating cutting-edge computational methodologies with advanced experimental characterization techniques is crucial for advancing a deeper and more fundamental understanding of HEM systems [211]. Widely utilized computational methods, including DFT and molecular dynamics (MD), have proven indispensable for investigating HEMs [154,211,212]. By evaluating parameters such as adsorbate binding energies, electronic states, electric field distributions, ion migration energies, and surface charge distributions, these approaches provide atomic-level insights into charge transfer and catalysis mechanisms, thereby accelerating the advancement of HEMs [164].

However, the intricate and numerous possible atomic

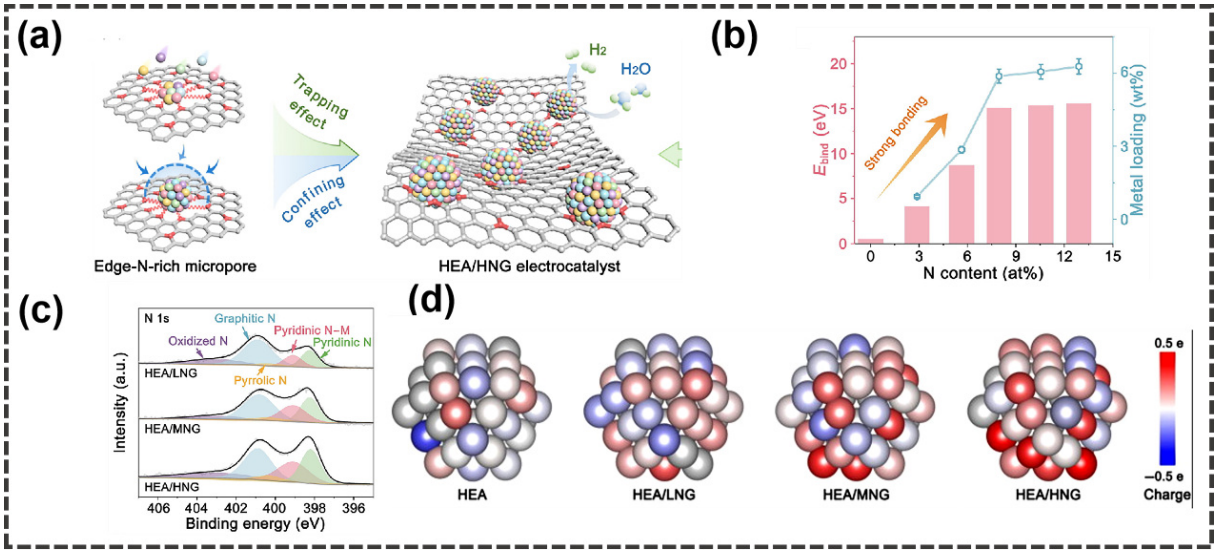

Fig. 6 Influence of support material selection on catalytic efficiency of HEMs. (a) Synthesis of PdPtRhIrRu HEA/HNG catalysts. (b) Theoretical calculations of binding energy alongside experimental mass loading of HEA on N-doped graphene with various N contents. (c) N 1s XPS spectra and (d) Bader charge distribution analysis of HEA systems supported by various materials. Reproduced with permission from Ref. [210], © Science China Press 2022.

configurations characteristic of high-entropy catalysts not only complicate composition optimization through conventional methods but also impose substantial burdens for computational screening. The advent of advanced computational technologies, such as high-throughput screening and machine learning (ML) algorithms, offers considerable potential for accelerating the discovery of novel catalytic materials [62]. These techniques enable the rapid identification of high-activity HEM electrocatalysts with optimal adsorption energies. Notably, the integration of these computational strategies can also efficiently pinpoint elemental combinations capable of forming stable single-phase solid solution HEAs, thereby facilitating the efficient discovery of optimal HEM compositions for catalytic applications [213]. Perumal *et al.* [214] leveraged a Bayesian optimization (BO)-driven ML model employing Gaussian process regression (GPR) to predict the optimal octonary compositions (Al, Sn, Co, Ni, Cu, Ir, Ce, and Rh) of high-entropy nanoparticles for the HER and OER. The GPR model, trained on an initial dataset of 70 experimental samples, iteratively proposed new compositions via the upper confidence bound (UCB) acquisition function over 200 iterations. Shapley additive explanation (SHAP) analysis revealed that the Rh, Cu, and Al contents significantly influenced HER activity, whereas t-stochastic neighbor embedding (t-SNE) was used to visualize compositional clustering for performance optimization. After 10 BO-guided experiments, the optimized catalyst achieved an exceptionally low overpotential of 12 mV at 10 mA·cm^{-2}, outperforming commercial Pt/C (16 mV). For the OER, initial ML predictions have shown limited accuracy, which is attributed to dynamic *in situ* activation processes disrupting composition–activity relationships. This finding underscores the need for expanded datasets and feature vector refinement.

As an example of this approach applied outside the field of catalysis, Rao *et al.* [215] introduced an active learning system for efficiently discovering HEAs via sparse experimental datasets (Fig. 7(a)). This iterative approach refines the experimental design on the basis of models trained with prior results, continuously improving the data quality (Fig. 7(b)). By systematically evaluating 17 novel alloys from millions of potential compositions, the team identified two high-entropy Invar alloys exhibiting remarkably low thermal expansion coefficients (TECs) of 2×10^{-6} K^{-1} at 300 K (Fig. 7(c)). Conclusively, active learning provides a method for comprehending the fundamental physics that governs the relationship between composition and properties and identifying new, promising compositions. Kim *et al.* [216] carried out detailed calculations of the elastic constants for an FCC AlCoCrFeNi HEA, focusing specifically on the influence of lattice distortion (Fig. 7(d)). They reported that incorporating lattice distortion effects into DFT models brings the calculated elastic constants closer to the experimental values (Fig. 7(e)).

Fu *et al.* [143] utilized advanced computational algorithms to systematically explore and identify optimal Pt-free element combinations for HEAs with favorable hydrogen binding energies, with a focus on metals from periods 4–6. From this comprehensive screening process, elements such as Fe, Co, Ni, Cu, Zn, Ga, Mo, Ru, Pd, Ag, Cd, In, Sn, and Au were selected for further investigation. HEA configurations featuring randomized atomic distributions were subsequently constructed and investigated via *ab initio* molecular dynamics (AIMD) simulations and DFT calculations. This automated process identified combinations with ΔG_{H^*} values near zero, which were subsequently analyzed and are depicted in the volcano plot shown in Fig. 7(f). Among the identified systems, the Pd–Mo–Ga combination emerges as a particularly promising candidate, exhibiting superior hydrogen binding energy compared with that of Pt. In this ternary system, the quaternary alloy PdMoGaIn exhibited the best performance. After the introduction of a fifth element, PdMoGaInNi is determined to be the most effective composition. These findings underscore the need for more precise simulation methods capable of providing theoretical guidance and predictions at the atomic and molecular scales, which will be instrumental in optimizing electrode design and exploring novel HEMs for future applications [164].

Despite the significant advancements in HEM-based electrocatalysts, the pursuit of novel strategies remains imperative to further increase the catalytic efficiency of HEMs and expedite their practical implementation. Although the compositional diversity of HEMs offers tremendous potential for designing high-performance catalysts, it simultaneously poses enduring challenges in identifying the optimal composition without exhaustive trial-and-error experiments. Thus, theoretical calculations are increasingly indispensable in the design of advanced electrocatalysts.

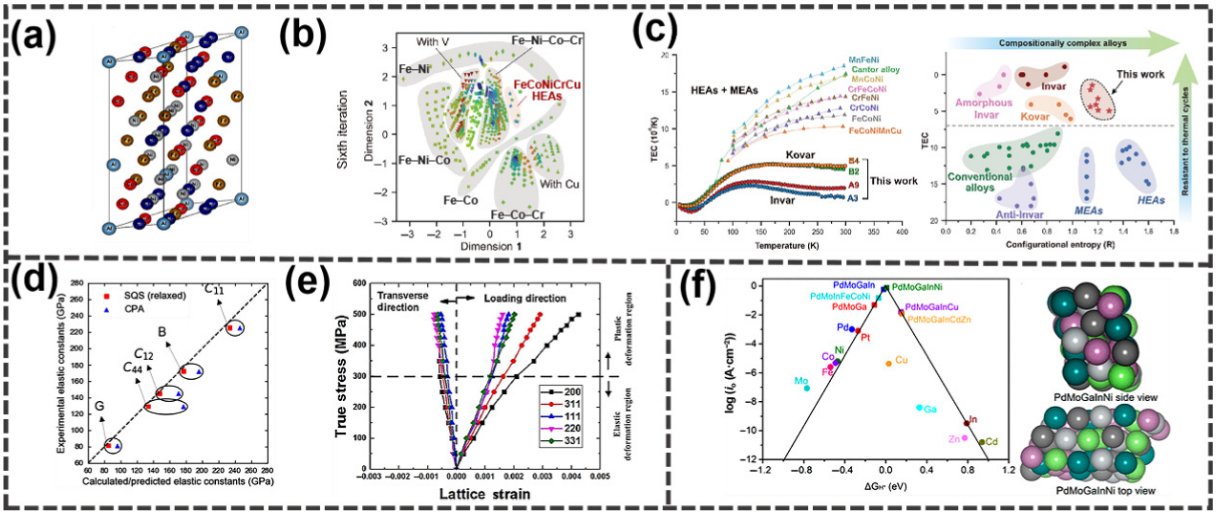

Fig. 7 Use of theoretical methods to identify routes to increase catalytic efficiency of HEMs. (a) A 64-atom special quasirandom structure (SQS) model was utilized for DFT calculations with labeled atomic species. (b) Latent space representation from a Wasserstein autoencoder (WAE). (c) TECs of machine-learning-optimized HEAs plotted as a function of temperature, alongside a plot of TEC vs. configurational entropy, showing that ML approach identified new complex compositions with low TECs. Reproduced with permission from Ref. [215], © 2022 The Authors, some rights reserved; exclusive licensee American Association for the Advancement of Science. (d) A comparative analysis of experimentally measured and theoretically calculated elastic constants and elastic moduli for FCC $Al_{0.3}CoCrFeNi$ HEA, which is based on SQS and coherent potential approximation (CPA) models. (e) Evolution of lattice strain in $Al_{0.3}CoCrFeNi$ HEA as a function of true stress. Reproduced with permission from Ref. [216], © Acta Materialia Inc. 2019. (f) Volcano plot of various Pt-free HEA compositions for HER, alongside side and top views of PdMoGaInNi, identified as the best HER catalyst. Reproduced with permission from Ref. [143], © American Chemical Society 2022.

3.8 Summary of optimization strategies for HEMs

To improve the electrocatalytic efficiency of HEMs, the primary focus is on simultaneously enhancing the inherent activity and increasing the density of active sites, which can be approached from several key perspectives: component design, reaction kinetics optimization, and electronic structure regulation. The component design mainly includes changes in the crystal structure and doping effects. The crystal structure of materials affects their catalytic performance. Notably, HEMs with an FCC structure exhibit higher density active site exposure and better electron transport capacity, rendering them more favorable for facilitating catalytic reactions. The doping strategy can improve the adsorption capacity and degree of activation of intermediates by adjusting the electron density and activation energy of catalysts. Additionally, the kinetics of catalytic reactions are often influenced by catalyst morphology. Among the diverse morphological architectures, porous layered configurations and ultrasmall nanostructures offer large specific surface areas and an abundance of exposed catalytically active sites, significantly improving catalytic efficiency. In addition, the adjustable electronic structures of HEMs are crucial for further improving their catalytic performance. Advanced design methodologies, such as strain modulation, defect tailoring, and conductive carrier integration, can induce charge redistribution across the HEM surface. This redistribution promotes selective electron accumulation or depletion, influencing the adsorption and desorption behavior of reaction intermediates. More importantly, shifts in the d-band center can alter the binding energies of adsorbates on the catalyst surface, thereby impacting the catalytic performance.

However, key challenges remain, including the development of effective synthesis strategies capable of precisely controlling surface and electronic structures to further enhance catalytic performance. Processing strategies for engineering the surfaces and internal electronic structure of HEM-based catalysts often involve complex, multistep procedures and costly instrumentation, presenting significant challenges in producing catalysts with precisely designed and controlled surfaces [217]. Consequently, further advancements in HEM processing are required to enable precise control over morphology, surface states, and electronic structure, along with the adoption of targeted strategies to simultaneously improve both their activity and stability. To advance the development and practical application of HEM-based catalysts, efforts are also needed to develop practical and scalable methods for the controlled large-scale fabrication of electrode materials.

Additionally, theoretical and computational methods can play a key role in optimizing HEM electrocatalysts, particularly in terms of understanding reaction mechanisms, tuning active sites to optimize intermediate binding strength at each reaction step, and guiding composition selection from the vast compositional space.

Furthermore, a comparative analysis of the differences between strategies aimed at enhancing catalyst stability and those aimed at improving activity was conducted, the results of which are presented in Table 3. According to Table 3, it can be concluded that activity enhancement strategies are focused primarily on improving the intrinsic reactivity of the active sites and the accessibility of the reactants. Specifically, by optimizing electronic structures (such as d-band center modulation and multielement synergy) and accelerating reaction kinetics (such as employing ultrasmall nanoparticles and constructing porous frameworks), these approaches aim to improve intermediate adsorption and maximize the exposure of active sites. In contrast, stability enhancement focuses on suppressing the degradation pathways of catalysts, including aggregation, leaching, and phase transformation.

4 Stability optimization

In addition to exhibiting high catalytic activity, stability is a critical parameter for heterogeneous catalysts, particularly in industrial applications [218,219]. HEMs generally exhibit exceptional stability, attributed to the high-entropy effect combined with synergistic interactions [95]. In contrast, commonly employed noble-metal-based catalysts, such as those derived from Pt, Au, and Ru, often exhibit inferior stability under catalytic conditions,

Table 3 Comparative analysis of optimization strategies for determining catalytic activity and stability of HEMs

Strategy	Activity enhancement mechanism	Stability enhancement mechanism
Composition regulation	Coordinated optimization of multiple active sites	High-entropy effect suppresses phase separation
Strain engineering	Regulating the adsorption strength of intermediates	Heterogeneous interfaces
Defect engineering	Increasing active sites and optimizing charge transfer	—
Morphology control	Increasing the exposure of active sites and enhancing atomic utilization	Preventing particle agglomeration
Support interaction	Enhancing electrical conductivity and optimizing charge transfer and redistribution	Strong interface anchoring to prevent particle detachment
Computational prediction	Exploring optimal composition	—

significantly restricting their industrial viability [220]. For example, Pt NPs frequently aggregate during the OER due to Ostwald ripening, resulting in a gradual decline in catalytic performance during extended operation [115]. Furthermore, in Pt-based binary or ternary alloys, the constituent metals are prone to leaching into the reaction medium, potentially compromising the structural integrity of the catalysts [98].

While the structural stability of HEMs is governed by the Gibbs energy of mixing, as described by Eq. (3). The high level of disorder existing in the distribution of elements maximizes entropy and maintains the materials in a stable state [221]. To further improve the stability of HEM catalysts, many strategies, such as conductive carrier loading, d-band center adjustment, size control, and element regulation, have been proposed. Recently, Gao *et al.* [222] prepared ultrasmall and highly distributed FeCoPdIrPt HEA-NPs on graphene oxide granular supports. The stability of the FeCoPdIrPt@GO catalyst was markedly enhanced because of the entropic stabilization, which produced a thermodynamically stable state and prevented the HEA-NPs from degrading. Zhang *et al.* [144] successfully synthesized a Pd-based HEA, specifically PdFeCoNiCu NPs, via the oil-phase method at relatively low temperatures (≤ 250 °C). The resulting nanoparticles had a small average size of approximately 34 nm, making them effective for the alkaline HER. Notably, when combined with carbon black, the PdFeCoNiCu/C electrocatalyst exhibited remarkable stability, maintaining its electroactivity even after continuous testing for half a month, and its structure was effectively preserved. DFT calculations indicate that Fe maintains considerable electrical activity throughout the HER process by promoting d–d electron coupling and compensating for electron deficiencies at Co sites. Moreover, Cu, as an electron-rich species, facilitates general electron transfer between metal sites. The stabilization of the electroactive Co sites is beneficial for water splitting, whereas neighboring Ni sites further stabilize *OH intermediates during the reaction.

Abdelhafiz *et al.* [148] investigated ternary to secondary HEO catalysts (converted from HEAs) deposited on carbon fiber substrates (Fig. 8(a)). The XRD patterns of a FeNiCoCr HEO after OER testing (Fig. 8(b)) reveal the emergence of new peaks and variations in the peak intensity ratio, indicating the presence of oxyhydroxide and carbide phases in addition to the original spinel phase and suggesting that the interfacial reconstruction of carbon atoms between the FeNiCoCr HEO nanoparticles and the carbon fiber substrate under reaction conditions facilitates the formation of carbide phases. Consequently, owing to the strong carbide-mediated intimate relationship between the HEO particles and the carbon substrate, the catalyst nanoparticles are mechanically stable. This is consistent with previous work that has shown high stability during the OER for single-atom catalysts on carbide supports [223].

To assess the stability of their electrocatalyst relative to recently reported counterparts, Kwon *et al.* [130] utilized the stability number (S-number), a standardized parameter for evaluating catalyst stability. The S-number, which represents the ratio of the generated gaseous product to the amount of dissolved catalyst, serves as an indicator of active site durability. As shown in Fig. 8(c), ZnNiCoIrMn results in significantly greater S-numbers for both the HER and OER when contrasted with ternary, quaternary, and other quinary systems, such as ZnNiCoIrFe. The remarkable stability can be ascribed to the high-entropy stabilization effect, which is fundamentally dictated by the thermodynamic principle $\Delta G_{mix} = \Delta H_{mix} - T\Delta S_{mix}$. The inherent lattice distortion, arising from variations in the lattice parameters of the constituent elements, leads to a sluggish diffusion phenomenon that mitigates element dissolution and improves stability. Moreover, the stability of the ZnNiCoIrMn HEA is strongly influenced by the specific alloying elements. For example, Mn incorporation results in superior stability compared with Fe incorporation in quinary HEAs, as evidenced in Fig. 8(d). This can be attributed to the fact that Mn has greater cohesive energy than Fe, which suppresses element dissolution (Fig. 8(e)). The dissolution of Ir, which has a high cohesive energy, is significantly affected by the adsorption energy of the oxygen species (ΔE_O). Metals with a higher ΔE_O are prone to forming thicker oxide layers during adsorption, generating uncoordinated metal sites upon desorption, thereby accelerating the dissolution of metallic species. The integration of Mn into the ZnNiCoIrMn alloy addresses this challenge by effectively suppressing the ΔE_O at the Ir sites. This suppression of Ir dissolution during the adsorption and desorption of oxygen intermediates underscores the critical role of Mn in enhancing stability [130].

In conclusion, the choice of appropriate HEM composition and support materials is imperative for achieving high stability and hence for the practical application of HEMs.

5 Conclusions and perspectives

HEMs have gained prominence as innovative catalysts for water electrolysis, offering unparalleled versatility in their compositions and structures, leading to catalysts with inherently high catalytic activity and exceptional stability. This paper focuses on design strategies aimed at developing high-performance and stable electrochemical HEMs for water splitting. Catalyst design strategies for improving HEM performance, such as component regulation, the introduction of defects, strain engineering, morphological engineering, and the use of conductive carrier supports, have been reviewed, alongside the role of computational methods in predicting optimal compositions. A comparison of different strategies for optimizing HEM catalysts is shown in Table 4.

Despite the achievements to date in HEM catalysis and successful improvement through various optimization strategies, there are still limitations and challenges. On one hand, HEMs

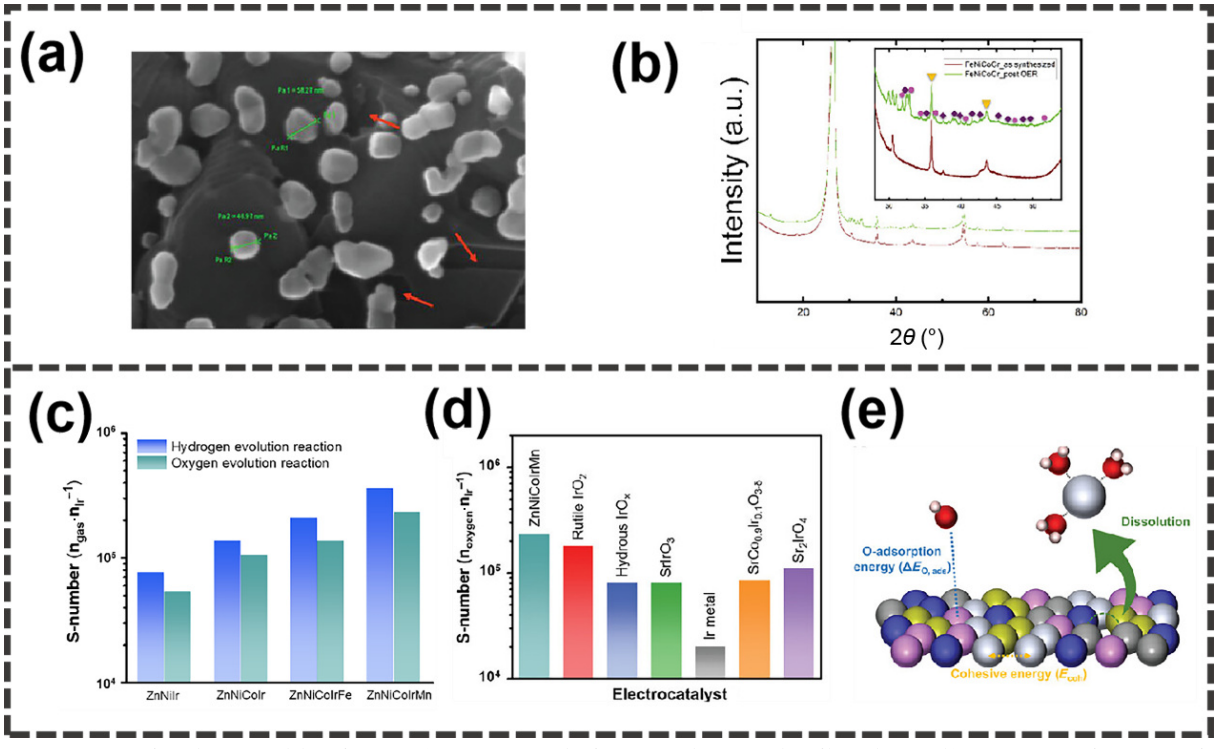

Fig. 8 Design strategies for enhancing stability of HEMs. (a) SEM micrograph of HEA particles on a carbon fiber substrate. (b) XRD patterns of FeNiCoCr after OER testing. Reproduced with permission from Ref. [148], © The Authors 2022. (c) S-number values of ZnNiIr-based electrocatalysts for HER and OER processes. (d) Comparative analysis of S-number for ZnNiCoIrMn with that of previously reported Ir-based catalysts. (e) Key factors influencing metal dissolution. Reproduced with permission from Ref. [130], © Wiley-VCH GmbH 2023.

possess intrinsic complexity due to their extensive compositional diversity and randomly mixed multielement structures, making their understanding and rational design extremely challenging. On the other hand, the targeted reactions are typically intricate and involve numerous intermediates and multiple reaction pathways. Consequently, research into HEM electrocatalysts for driving the HER and OER remains in its early stages, presenting both significant opportunities and considerable challenges, as shown in Fig. 9:

(1) Rational element selection. The selection of elements is initially informed by their intrinsic activity in specific catalytic processes. Subsequent optimization can then be achieved by tailoring the electronic structure of the HEMs, including adjusting the d-band center and charge transfer characteristics. By tuning the elemental composition and concentration, it is possible to modulate the d-band center, thereby influencing the catalytic activity. Additionally, electron transfer between distinct elements induces surface charge redistribution, which subsequently governs the adsorption behavior of reactants and intermediates at the active sites. In addition, element selection is also important because it governs the amount of lattice strain. This is primarily due to the differences in the atomic radii, electronegativity, and bonding characteristics between the chosen elements. When elements with significantly different atomic sizes are introduced into a crystal lattice, they can cause local distortions and strain, as the lattice adjusts to accommodate the size mismatch. Optimal element combinations balance lattice distortion, chemical compatibility, and synergistic effects to achieve enhanced catalytic activity and stability. Thus, strategic element selection is vital for enhancing the performance of HEMs. Furthermore, it is essential to evaluate the compatibility of elements, with particular emphasis on the feasibility of forming a homogeneous single-phase solid solution or compound under defined conditions. Through the systematic analysis of physical and chemical parameters, such as the atomic radii, electronegativities, and valence electron configurations, as well as the mixing enthalpy and entropy, it becomes possible to predict the optimal element combinations. This approach provides a robust foundation for strategic material design.

(2) Advanced characterization techniques. A comprehensive grasp of the complex connection between the structure and catalytic performance of HEMs is essential for advancing highly efficient catalysts. This relationship is further obscured by the inherent complexity of redox processes, necessitating the use of advanced high-resolution *in situ* characterization techniques. These methods are invaluable for tracking structural evolution and elucidating reaction mechanisms. In particular, *in situ* techniques enable the evaluation of the stability and dynamic monitoring of interface evolution. By integrating multiple characterization approaches, particularly *in situ* methods, surfaces and interfaces, and their evolution during reactions can be comprehensively analyzed in terms of morphology, composition, structure, and chemical environment, revealing both surface active sites and structural features. Consequently, the advancement of more sophisticated *in situ* approaches is indispensable for unraveling the behavior of HEM catalysts during electrocatalytic processes.

(3) Indispensable theoretical and computational techniques. HEMs have gained recognition as potential candidates for efficient electrocatalysis, driving intensive research efforts to identify active centers and optimal compositions. Theoretical modeling has proven to be invaluable for probing the electronic properties of catalysts, alongside elucidating reaction intermediates and mechanisms. With advances in computational methods, simulation and modeling tools are increasingly being utilized to predict the structure formation rules and attributes of HEMs, thus

Table 4 Comparison of different strategies for optimizing HEM catalysts

Material	Optimization strategy	Advantage	Disadvantage	Ref.
$Pt_{34}Fe_5Ni_{20}Cu_{31}Mo_9Ru$	Composition regulation	Nanocrystals with high-index facets	Regulating the atomic arrangement with a chemically ordered distribution and optimizing structural site-isolation effects	[140]
FeCoNiCu	Morphology control	Porous morphology offers an effective surface area and accelerates charge transport dynamics	Controlling ligament size length and mesopore diameters	[136]
FeCoNiRu		The hollow active sites allow for the fast charge transfer and mitigate the growth of nanoparticles	Considering agglomeration phenomenon and ensuring the integrity of carbon skeleton	[137]
NiCoFePtRh		Ultrasmall nanostructure can afford ultrahigh atom utilization	Being difficult to control synthesis of ultrafine HEA NPs without separate phases	[195]
P–$Ni_{30}Co_{30}Fe_{10}Cr_{10}Al_{18}W_2$	Doping	P doping-induced lattice strain	The incorporation of anions into transition metals typically results in the creation of their compounds	[131]
V_xCuCoNiFeMn		The V incorporation can increase active sites	Optimizing the mole fraction of V in CuCoNiFeMn HEA within an appropriate range	[152]
ZnNiCoIrMn	Electronic structure	d-band center downshifting weakens adsorption energy	Preventing elements dissolution into corrosive solutions	[130]
FeCoNiMnRu	Electronegativity difference	The electronegativity differences induce charge redistribution	Accurately identifying active centers and activity origins	[128]
FeCoNiCuMn		The local electron interaction among multiple metal sites caused by electronegativity differences	Excessive or insufficient molecular adsorption can result in a reduction in catalytic activity	[108]
$(FeCoNiB_{0.75})_{97}Pt_3$	Defects	Optimizing atomic configuration and modulating electronic interaction	Focusing on strategies to optimize surface defects in materials for enhanced electrocatalytic performance	[182]
FeCoNiCrCu	Theoretical prediction	Determining the optimal combination through active learning calculation	Considering compositional information rather than the alloy production process	[132]
$Al_{0.3}$CoCrFeNi		Studying the correlation between the elastic properties and lattice distortion	Being difficult to construct subminiature cell models	[219]
PdMoGaInNi		Determining the optimal combination via computer-facilitated screening	The alloying strategy remains restricted by conventional synthesis techniques	[148]
PdPtRhIrRu/N–C	Carrier supports	Promoting the optimization of the electronic states of metal	Adjustment of the electronic state of metal centers	[210]

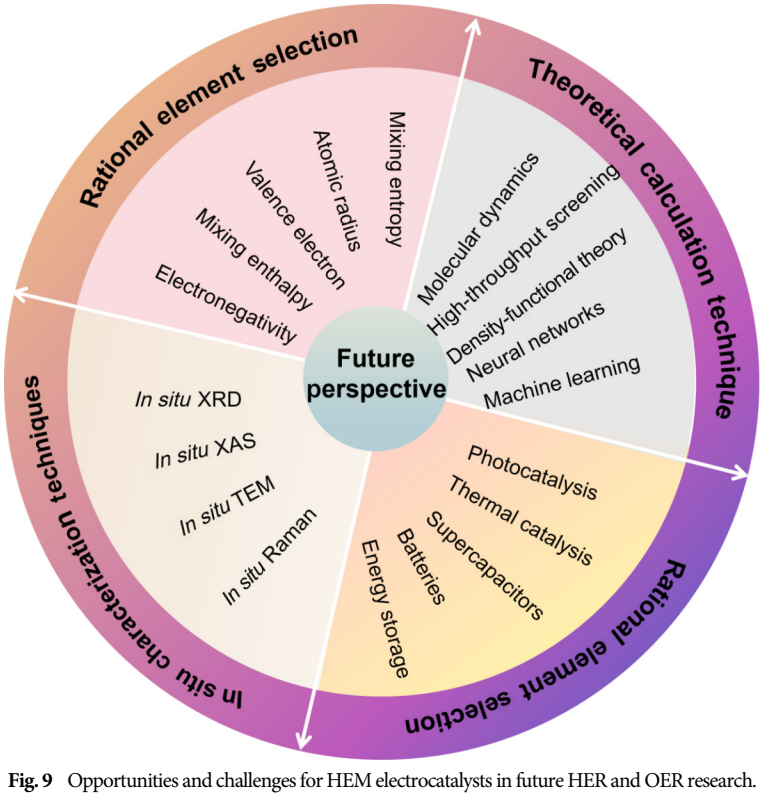

Fig. 9 Opportunities and challenges for HEM electrocatalysts in future HER and OER research.

guiding efficient exploration of the vast HEM compositional space. Innovative computational techniques, including DFT, molecular dynamics, machine learning, and neural networks, have significantly advanced the identification and evaluation of active sites and expedited insights into adsorption energy modulation as a function of HEM composition and structure. Consequently, an integrative strategy that fuses theoretical modeling with experimental validation is crucial for driving the continued progress of HEM electrocatalysts.

(4) Extension of applications. While research into HEM catalysts is still at an early stage, they hold tremendous potential across a broad array of applications, including not only electrocatalytic water splitting, which has been the focus of this review, but also electrocatalysis of other reactions, as well as photocatalysis, thermal catalysis, supercapacitors, energy storage, and batteries. The unique structural characteristics and vast compositional versatility of HEMs offer opportunities to advance all of these applications. Future research should focus on designing novel compositions and structures tailored to each specific application, alongside improving the fundamental understanding of how HEMs function. Such efforts will be critical for unlocking their superior performance across a wide range of fields. Interdisciplinary approaches—such as integrating HEMs with photoelectrochemical systems or employing atomic layer deposition (ALD) for precise surface engineering—will be essential to overcome existing challenges. Furthermore, the concept of HEMs has broadened to encompass a diverse array of systems, such as high-entropy metal organic frameworks, MXenes, oxides (e.g., perovskites and spinels), fluorides, borides, phosphides, and nitrides. While these materials hold significant potential across diverse fields, their role in emerging applications (e.g., CO_2 reduction and biomass valorization) merits focused exploration. Further research is needed to explore their applications and capabilities.

Acknowledgements

Wenxian Li acknowledges financial support from an Australian Research Council Future Fellowship (No. FT230100436), the Australian Research Council Centre of Excellence for Carbon Science and Innovation (CE230100032), BAJC R&D project (Nos. BA23011 and BA24010), the IH230100010 ARC Hub-BAJC Project (No. SPDC-P09), and the UNSW Science Translational Impact Seed Funding. Bin Liu acknowledges research support from the Shanghai Technical Service Center for Advanced Ceramics Structure Design and Precision Manufacturing (No. 20DZ2294000).

Availability of data and materials

The data are available from the corresponding author upon reasonable request.

Competing interests

The authors have no competing interests to declare that are relevant to the content of this article. The authors Bin Liu and Wenxian Li are Editorial Committee members of this journal.

References

[1] Ge RY, Huo JJ, Liao T, *et al.* Hierarchical molybdenum phosphide coupled with carbon as a whole pH-range electrocatalyst for hydrogen evolution reaction. *Appl Catal B Environ* 2020, **260**: 118196.

[2] Thalluri SM, Bai LC, Lv CC, *et al.* Strategies for semiconductor/electrocatalyst coupling toward solar-driven water splitting. *Adv Sci* 2020, **7**: 1902102.

[3] Chen YC, Lu AY, Lu P, *et al.* Structurally deformed MoS_2 for electrochemically stable, thermally resistant, and highly efficient hydrogen evolution reaction. *Adv Mater* 2017, **29**: 1703863.

[4] Yuan S, Zhao CF, Cai XY, *et al.* Bubble evolution and transport in PEM water electrolysis: Mechanism, impact, and management. *Prog Energ Combust* 2023, **96**: 101075.

[5] Ge RY, Huo JJ, Sun MJ, *et al.* Surface and interface engineering: Molybdenum carbide-based nanomaterials for electrochemical energy conversion. *Small* 2021, **17**: 1903380.

[6] Sheng HY, Janes AN, Ross RD, *et al.* Linear paired electrochemical valorization of glycerol enabled by the electro-Fenton process using a stable $NiSe_2$ cathode. *Nat Catal* 2022, **5**: 716–725.

[7] Song HJ, Yoon H, Ju B, *et al.* Highly efficient perovskite-based electrocatalysts for water oxidation in acidic environments: A mini review. *Adv Energy Mater* 2021, **11**: 2002428.

[8] Huang HJ, Yan MM, Yang CZ, *et al.* Graphene nanoarchitectonics: Recent advances in graphene-based electrocatalysts for hydrogen evolution reaction. *Adv Mater* 2019, **31**: 1903415.

[9] Yu HJ, Wei XD, Wang M, *et al.* Macroscopic polarization enhancement boosting piezo-photocatalytic performance via Nb-doping on B-site of $Bi_4Ti_3O_{12}$ nanosheets. *J Adv Ceram* 2024, **13**: 437–446.

[10] Zhou SF, Wang JT, Li J, *et al.* Surface-growing organophosphorus layer on layered double hydroxides enables boosted and durable electrochemical freshwater/seawater oxidation. *Appl Catal B Environ* 2023, **332**: 122749.

[11] Poudel MB, Logeshwaran N, Prabhakaran S, *et al.* Low-cost hydrogen production from alkaline/seawater over a single-step synthesis of Mo_3Se_4–NiSe core–shell nanowire arrays. *Adv Mater* 2024, **36**: 2305813.

[12] Pattaweepaiboon S, Samarungkasut P, Iamprasertkun P, *et al.* Single-atom to ultrasmall Au nanoparticles anchored on NiFe layered double hydroxide as catalyst for oxygen and hydrogen evolution reactions. *ACS Appl Nano Mater* 2025, **8**: 438–448.

[13] Xu Y, Qu JT, Li Y, *et al.* Bridging metal-ion induced vertical growth of MoS_2 and overall fast electron transfer in $(C,P)_3N_4$–$M(Ni^{2+},Co^{2+})$–MoS_2 electrocatalyst for efficient hydrogen evolution reaction. *Sustain Mater Technol* 2020, **25**: 00172.

[14] Wang Y, *et al.* Mesoporous single-crystalline particles as robust and efficient acidic oxygen evolution catalysts. *J Am Chem Soc* 2025, **147**: 13345–13355.

[15] Wang Y, Xu XL, Xiao LB, *et al.* Balancing the piezoelectric coefficient and carrier concentration of Bi_2WO_{6-x} for ultrahigh piezocatalysis. *J Adv Ceram* 2024, **13**: 1737–1747.

[16] Huo JJ, Chen YL, Liu Y, *et al.* Bifunctional iron nickel phosphide nanocatalysts supported on porous carbon for highly efficient overall water splitting. *Sustain Mater Technol* 2019, **22**: 00117.

[17] Landman A, Hadash S, Shter GE, *et al.* High performance core/shell Ni/$Ni(OH)_2$ electrospun nanofiber anodes for decoupled water splitting. *Adv Funct Mater* 2021, **31**: 2008118.

[18] Liu HB, Li JC, Zhang YQ, *et al.* Boosted water electrolysis capability of Ni_xCo_yP via charge redistribution and surface activation. *Chem Eng J* 2023, **473**: 145397.

[19] Cheng ZH, Xiao YK, Wu WP, *et al.* All-pH-tolerant in-plane heterostructures for efficient hydrogen evolution reaction. *ACS Nano* 2021, **15**: 11417–11427.

[20] Lin YC, Dong Y, Wang XZ, *et al.* Electrocatalysts for the oxygen evolution reaction in acidic media. *Adv Mater* 2023, **35**: 2210565.

[21] Jhu PS, Chang CW, Cheng CC, *et al.* Non-precious high entropy alloys and highly alkali-resistant composite membranes based high performance anion exchange membrane water electrolyzers. *Nano Energy* 2024, **126**: 109703.

[22] Xu Y, Kraft M, Xu R. Metal-free carbonaceous electrocatalysts and photocatalysts for water splitting. *Chem Soc Rev* 2016, **45**: 3039–3052.

[23] Wang Y, Ni M, Yan W, *et al.* Supported high-entropy alloys for

electrooxidation of benzyl alcohol assisted water electrolysis. *Adv Funct Mater* 2024, **34**: 2311611.
[24] Wang PY, Zhu JW, Pu ZH, *et al.* Interfacial engineering of Co nanoparticles/Co_2C nanowires boosts overall water splitting kinetics. *Appl Catal B Environ* 2021, **296**: 120334.
[25] Chen ZL, Qing HL, Zhou K, *et al.* Metal–organic framework-derived nanocomposites for electrocatalytic hydrogen evolution reaction. *Prog Mater Sci* 2020, **108**: 100618.
[26] Hong YR, Kim KM, Ryu JH, *et al.* Dual-phase engineering of nickel boride-hydroxide nanoparticles toward high-performance water oxidation electrocatalysts. *Adv Funct Mater* 2020, **30**: 2004330.
[27] Chen JB, Ying J, Xiao YX, *et al.* Directed mass and electron transfer promoted by hierarchical porous Co–P–O leads to enhancement of the overall water splitting efficiency. *ACS Catal* 2023, **13**: 14802–14812.
[28] Zhao ZH, Schipper DE, Leitner AP, *et al.* Bifunctional metal phosphide FeMnP films from single source metal organic chemical vapor deposition for efficient overall water splitting. *Nano Energy* 2017, **39**: 444–453.
[29] Rong W, Chen YF, Dang R, *et al.* Amorphous high-entropy $IrRuCrFeCoNiO_x$ as efficient water splitting oxygen evolution reaction electrocatalysts. *J Alloys Compd* 2024, **971**: 172786.
[30] Haq TU, Haik YA roadmap towards sustainable anode design for alkaline water electrolysis. *Appl Catal B Environ* 2023, **334**: 122853.
[31] Yu MQ, Budiyanto E, Tüysüz H. Principles of water electrolysis and recent progress in cobalt-, nickel-, and iron-based oxides for the oxygen evolution reaction. *Angew Chem-Ger Edit* 2022, **134**: 202103824.
[32] Zaman WQ, Sun W, Tariq M, *et al.* Iridium substitution in nickel cobaltite renders high mass specific OER activity and durability in acidic media. *Appl Catal B Environ* 2019, **244**: 295–302.
[33] Li JY, Yan M, Zhou XM, *et al.* Mechanistic insights on ternary $Ni_{2-x}Co_xP$ for hydrogen evolution and their hybrids with graphene as highly efficient and robust catalysts for overall water splitting. *Adv Funct Mater* 2016, **26**: 6785–6796.
[34] Wang J, Kong H, Zhang JY, *et al.* Carbon-based electrocatalysts for sustainable energy applications. *Prog Mater Sci* 2021, **116**: 100717.
[35] Han JY, Deng NP, Chi H, *et al.* Recent advances of carbon fiber-based self-supported electrocatalysts in oxygen electrocatalysis. *J Energy Chem* 2024, **98**: 334–363.
[36] Yu MZ, Wang ZY, Liu JS, *et al.* A hierarchically porous and hydrophilic 3D nickel–iron/MXene electrode for accelerating oxygen and hydrogen evolution at high current densities. *Nano Energy* 2019, **63**: 103880.
[37] Wang XS, Zheng Y, Sheng WC, *et al.* Strategies for design of electrocatalysts for hydrogen evolution under alkaline conditions. *Mater Today* 2020, **36**: 125–138.
[38] Zhao HF, Yao JQ, Wang YS, *et al.* Crystal facets-activity correlation for oxygen evolution reaction in compositional complex alloys. *Adv Sci* 2024: 2404095.
[39] Li SS, Gao YQ, Li N, *et al.* Transition metal-based bimetallic MOFs and MOF-derived catalysts for electrochemical oxygen evolution reaction. *Energy Environ Sci* 2021, **14**: 1897–1927.
[40] Luo MC, Zhao ZL, Zhang YL, *et al.* PdMo bimetallene for oxygen reduction catalysis. *Nature* 2019, **574**: 81–85.
[41] Li WX, Liu Y, Azam A, *et al.* Unlocking efficiency: Minimizing energy loss in electrocatalysts for water splitting. *Adv Mater* 2024: 2404658.
[42] Huang MJ, Yang HY, Xia X, *et al.* Highly active and robust Ir–Ru electrocatalyst for alkaline HER/HOR: Combined electronic and oxophilic effect. *Appl Catal B-Environ* 2024, **358**: 124422.
[43] Liu N, Lu YK, Hao HY, *et al.* Ring-shaped cavity anchor Pt to derive Pt/WO_{3-x} heterointerfaces for efficient hydrogen evolution in acidic water and seawater. *J Colloid Interf Sci* 2024, **676**: 918–926.
[44] Huang ZP, Chen ZZ, Chen ZB, *et al.* Cobalt phosphide nanorods as an efficient electrocatalyst for the hydrogen evolution reaction. *Nano Energy* 2014, **9**: 373–382.
[45] Wei M, Sun YY, Ai F, *et al.* Stretchable high-entropy alloy nanoflowers enable enhanced alkaline hydrogen evolution catalysis. *Appl Catal B Environ* 2023, **334**: 122814. 8.
[46] Xie HP, Zhao ZY, Liu T, *et al.* A membrane-based seawater electrolyser for hydrogen generation. *Nature* 2022, **612**: 673–678.
[47] Yang HY, Chen ZL, Guo PF, *et al.* B-doping-induced amorphization of LDH for large-current-density hydrogen evolution reaction. *Appl Catal B Environ* 2020, **261**: 118240.
[48] Jiang ZH, Zhang QY. The structure of glass: A phase equilibrium diagram approach. *Prog Mater Sci* 2014, **61**: 144–215.
[49] Schuler T, Kimura T, Schmidt TJ, *et al.* Towards a generic understanding of oxygen evolution reaction kinetics in polymer electrolyte water electrolysis. *Energ Environ Sci* 2020, **13**: 2153–2166.
[50] Wang K, Huang JH, Chen HX, *et al.* Recent progress in high entropy alloys for electrocatalysts. *Electrochem Energy Rev* 2022, **5**: 17.
[51] Yeh JW, Chen SK, Lin SJ, *et al.* Nanostructured high-entropy alloys with multiple principal elements: Novel alloy design concepts and outcomes. *Adv Eng Mater* 2004, **6**: 299–303.
[52] Cantor B, Chang ITH, Knight P, *et al.* Microstructural development in equiatomic multicomponent alloys. *Mater Sci Eng A* 2004, **375–377**: 213–218.
[53] George EP, Raabe D, Ritchie RO. High-entropy alloys. *Nat Rev Mater* 2019, **4**: 515–534.
[54] Wang R, Huang JZ, Zhang XH, *et al.* Two-dimensional high-entropy metal phosphorus trichalcogenides for enhanced hydrogen evolution reaction. *ACS Nano* 2022, **16**: 3593–3603.
[55] Ma YJ, Ma Y, Wang QS, *et al.* High-entropy energy materials: Challenges and new opportunities. *Energ Environ Sci* 2021, **14**: 2883–2905.
[56] Lee CH, Chou Y, Kim G, *et al.* Lattice-distortion-enhanced yield strength in a refractory high-entropy alloy. *Adv Mater* 2020, **32**: 2004029.
[57] Liu Y, Rong XH, Bai R, *et al.* Identifying the intrinsic anti-site defect in manganese-rich NASICON-type cathodes. *Nat Energy* 2023, **8**: 1088–1096.
[58] Li KX, He JF, Guan XZ, *et al.* Phosphorus-modified amorphous high-entropy CoFeNiCrMn compound as high-performance electrocatalyst for hydrazine-assisted water electrolysis. *Small* 2023, **19**: 2302130.
[59] Bao C, Chu P, Xu CX, *et al.* More disorder is better: Cutting-edge progress of high entropy materials in electrochemical energy storage applications. *Energy Storage Mater* 2024, **69**: 103408.
[60] Tang Y, Wang RX, Xiao B, *et al.* A review on the dynamic-mechanical behaviors of high-entropy alloys. *Prog Mater Sci* 2023, **135**: 101090.
[61] Zhong MX, Xu TT, Wang CXZ, *et al.* Utilizing high entropy oxide $(Ni_{0.2}Co_{0.2}Ca_{0.2}Cu_{0.2}Mg_{0.2})Fe_2O_4$ in chemical looping process for highly efficient and stable hydrogen production. *Chem Eng J* 2024, **487**: 150521.
[62] Li HD, Lai JP, Li ZJ, *et al.* Multi-sites electrocatalysis in high-entropy alloys. *Adv Funct Mater* 2021, **31**: 2106715.
[63] Li YG, Bai XH, Yuan DC, *et al.* Cu-based high-entropy two-dimensional oxide as stable and active photothermal catalyst. *Nat Commun* 2023, **14**: 3171.
[64] Ren JT, Chen L, Wang HY, *et al.* High-entropy alloys in electrocatalysis: From fundamentals to applications. *Chem Soc Rev* 2023, **52**: 8319–8373.
[65] Jing ZK, Guo YK, Wang Q, *et al.* Ambient hydrogenation of solid aromatics enabled by a high entropy alloy nanocatalyst. *Nat Commun* 2024, **15**: 5806.
[66] Xu WX, Zhang D, Wang TT, *et al.* Non-platinum-based electrocatalysts for high performance acidic hydrogen evolution reactions in proton exchange membrane water electrolysis. *Appl Catal B Environ* 2025, **361**: 124626.
[67] Gao GL, Sun ZX, Chen XL, *et al.* Recent advances in Ru/Ir-based electrocatalysts for acidic oxygen evolution reaction. *Appl Catal B Environ* 2024, **343**: 123584.

[68] Sivanantham A, Lee H, Hwang SW, *et al.* Preparation, electrical and electrochemical characterizations of CuCoNiFeMn high-entropy-alloy for overall water splitting at neutral-pH. *J Mater Chem A* 2021, **9**: 16841–16851.
[69] Cui MJ, Yang CP, Li BY, *et al.* High-entropy metal sulfide nanoparticles promise high-performance oxygen evolution reaction. *Adv Energy Mater* 2021, **11**: 2002887.
[70] Pei YH, Li D, Qiu CT, *et al.* High-entropy sulfide catalyst boosts energy-saving electrochemical sulfion upgrading to thiosulfate coupled with hydrogen production. *Angew Chem Int Ed* 2024, **63**: 202411977.
[71] Zhai YY, Ren XR, Wang BL, *et al.* High-entropy catalyst—A novel platform for electrochemical water splitting. *Adv Funct Mater* 2022, **32**: 2207536.
[72] Dai WJ, Lu T, Pan Y. Novel and promising electrocatalyst for oxygen evolution reaction based on MnFeCoNi high entropy alloy. *J Power Sources* 2019, **430**: 104–111.
[73] Huang K, Zhang BW, Wu JS, *et al.* Exploring the impact of atomic lattice deformation on oxygen evolution reactions based on a sub-5 nm pure face-centred cubic high-entropy alloy electrocatalyst. *J Mater Chem A* 2020, **8**: 11938–11947.
[74] Lai DW, Kang QL, Gao F, *et al.* High-entropy effect of a metal phosphide on enhanced overall water splitting performance. *J Mater Chem A* 2021, **9**: 17913–17922.
[75] Lei YT, Zhang LL, Xu WJ, *et al.* Carbon-supported high-entropy Co–Zn–Cd–Cu–Mn sulfide nanoarrays promise high-performance overall water splitting. *Nano Res* 2022, **15**: 6054–6061.
[76] Bo LL, Fang JY, Yang SB, *et al.* Modulating electron structure of active sites in high-entropy metal sulfide nanoparticles with greatly improved electrocatalytic performance for oxygen evolution reaction. *Int J Hydrog Energ* 2024, **84**: 89–96.
[77] Liao SX, Huang TQ, Wu WY, *et al.* Engineering high-entropy duel-functional nanocatalysts with regulative oxygen vacancies for efficient overall water splitting. *Chem Eng J* 2023, **471**: 144506.
[78] Wang H, He QF, Gao X, *et al.* Multifunctional high entropy alloys enabled by severe lattice distortion. *Adv Mater* 2024, **36**: 2305453.
[79] Qiu HJ, Fang G, Wen YR, *et al.* Nanoporous high-entropy alloys for highly stable and efficient catalysts. *J Mater Chem A* 2019, **7**: 6499–6506.
[80] Ahmad A, Nairan A, Feng Z, *et al.* Unlocking the potential of high entropy alloys in electrochemical water splitting: A review. *Small* 2024, **20**: 2311929.
[81] Li SR, Gong JL. Strategies for improving the performance and stability of Ni-based catalysts for reforming reactions. *Chem Soc Rev* 2014, **43**: 7245–7256.
[82] Hughes JP, Clipsham J, Chavushoglu H, *et al.* Polymer electrolyte electrolysis: A review of the activity and stability of non-precious metal hydrogen evolution reaction and oxygen evolution reaction catalysts. *Renew Sust Energy Rev* 2021, **139**: 110709.
[83] Nguyen TX, Su YH, Lin CC, *et al.* Self-reconstruction of sulfate-containing high entropy sulfide for exceptionally high-performance oxygen evolution reaction electrocatalyst. *Adv Funct Mater* 2021, **31**: 2106229.
[84] Hao YX, Yu DS, Zhu SQ, *et al.* Methanol upgrading coupled with hydrogen product at large current density promoted by strong interfacial interactions. *Energ Environ Sci* 2023, **16**: 1100–1110.
[85] Lin YH, Xu WC, Gao ZH, *et al.* Self-supporting high-entropy Co–Cr–Fe–Ni–Nb oxide electrocatalyst with nanoporous structure for oxygen evolution reaction. *Chem Eng J* 2024, **489**: 151233.
[86] Nandan R, Nara H, Nam HN, *et al.* Tailored design of mesoporous nanospheres with high entropic alloy sites for efficient redox electrocatalysis. *Adv Sci* 2024, **11**: 2402518.
[87] Yao RQ, Zhou YT, Shi H, *et al.* Nanoporous surface high-entropy alloys as highly efficient multisite electrocatalysts for nonacidic hydrogen evolution reaction. *Adv Funct Mater* 2021, **31**: 2009613.
[88] Qiu HJ, Fang G, Gao JJ, *et al.* Noble metal-free nanoporous high-entropy alloys as highly efficient electrocatalysts for oxygen evolution reaction. *ACS Mater Lett* 2019, **1**: 526–533.
[89] Lee SA, Bu J, Lee J, *et al.* High-entropy nanomaterials for advanced electrocatalysis. *Small Sci* 2023, **3**: 2200109.
[90] Huang J, Wang PL, Li P, *et al.* Regulating electrolytic $Fe_{0.5}$CoNiCuZn high entropy alloy electrodes for oxygen evolution reactions in alkaline solution. *J Mater Sci Technol* 2021, **93**: 110–118.
[91] Chang R, Li HD, Tian XF, *et al. In situ*, rapid synthesis of carbon-loaded high density and ultrasmall high entropy oxide nanoparticles as efficient electrocatalysts. *Small* 2024, **20**: 2309937.
[92] Fu H, Jiang Y, Zhang MZ, *et al.* High-entropy rare earth materials: Synthesis, application and outlook. *Chem Soc Rev* 2024, **53**: 2211–2247.
[93] Wang QS, Liu XW, He DP, *et al.* Fundamental comprehension, synthetic procedures and catalytic applications of high entropy oxide nanomaterials. *Mater Today* 2023, **70**: 218–236.
[94] Miracle DB, Senkov ON. A critical review of high entropy alloys and related concepts. *Acta Mater* 2017, **122**: 448–511.
[95] Zhou YB, Shen XW, Wang MF, *et al.* The understanding, rational design, and application of high-entropy alloys as excellent electrocatalysts: A review. *Sci China Mater* 2023, **66**: 2527–2544.
[96] Zhang WR, Liaw PK, Zhang Y. Science and technology in high-entropy alloys. *Sci China Mater* 2018, **61**: 2–22.
[97] Cantor B. Multicomponent high-entropy cantor alloys. *Prog Mater Sci* 2021, **120**: 100754.
[98] Wang Y, Luo WH, Gong S, *et al.* Synthesis of high-entropy-alloy nanoparticles by a step-alloying strategy as a superior multifunctional electrocatalyst. *Adv Mater* 2023, **35**: 2302499.
[99] Pan YT, Liu JX, Tu TZ, *et al.* High-entropy oxides for catalysis: A diamond in the rough. *Chem Eng J* 2023, **451**: 138659.
[100] Albedwawi SH, AlJaberi A, Haidemenopoulos GN, *et al.* High entropy oxides-exploring a paradigm of promising catalysts: A review. *Mater Design* 2021, **202**: 109534.
[101] Zhou YB, Shen XW, Qian T, *et al.* A review on the rational design and fabrication of nanosized high-entropy materials. *Nano Res* 2023, **16**: 7874–7905.
[102] Li XM, Zhou YF, Feng CR, *et al.* High entropy materials based electrocatalysts for water splitting: Synthesis strategies, catalytic mechanisms, and prospects. *Nano Res* 2023, **16**: 4411–4437.
[103] Li YO, Wang K, Wang XM, *et al.* Rare earth-incorporated high entropy oxides for energy and environmental catalysis. *Chinese J Catal* 2024, **61**: 54–70.
[104] Liu XF, Wang XY, Yang BB, *et al.* High-entropy layered oxides nanosheets for highly efficient photoelectrocatalytic reduction of CO_2 and application research. *Nano Res* 2023, **16**: 4775–4785.
[105] Cao JY, Xue YT, Ji ZY, *et al.* CoNi hexacyanoferrate nanoparticles anchored on carbon nanotubes as superior cathode materials for rechargeable aqueous zinc-ion batteries. *J Energy Storage* 2024, **86**: 111413.
[106] Nguyen TX, Su YH, Lin CC, *et al.* A new high entropy glycerate for high performance oxygen evolution reaction. *Adv Sci* 2021, **8**: 2002446.
[107] Sha SM, Ge RY, Li Y, *et al.* High-entropy catalysts for electrochemical water-electrolysis of hydrogen evolution and oxygen evolution reactions. *Front Energy* 2024, **18**: 265–290.
[108] Hao JC, Zhuang ZC, Cao KC, *et al.* Unraveling the electronegativity-dominated intermediate adsorption on high-entropy alloy electrocatalysts. *Nat Commun* 2022, **13**: 2662.
[109] Xin Y, Li SH, Qian YY, *et al.* High-entropy alloys as a platform for catalysis: Progress, challenges, and opportunities. *ACS Catal* 2020, **10**: 11280–11306.
[110] Mao QQ, Mu X, Deng K, *et al.* Multisite synergism-induced electron regulation of high-entropy alloy metallene for boosting alkaline hydrogen evolution reaction. *Adv Funct Mater* 2023, **33**: 2304963.
[111] Wang DD, Chen ZW, Huang YC, *et al.* Tailoring lattice strain in ultra-fine high-entropy alloys for active and stable methanol oxidation. *Sci China Mater* 2021, **64**: 2454–2466.
[112] Sun MJ, Ge RY, Li SA, *et al.* The component-activity interrelationship of cobalt-based bifunctional electrocatalysts for

overall water splitting: Strategies and performance. *J Energy Chem* 2024, **91**: 453–474.
[113] Zhang LJ, Cai WW, Bao NZ, *et al.* Implanting an electron donor to enlarge the d-p hybridization of high-entropy (oxy)hydroxide: A novel design to boost oxygen evolution. *Adv Mater* 2022, **34**: 2110511.
[114] Jin ZY, Lyu J, Zhao YL, *et al.* Top–down synthesis of noble metal particles on high-entropy oxide supports for electrocatalysis. *Chem Mater* 2021, **33**: 1771–1780.
[115] Zeng KZ, Zhang JW, Gao WQ, *et al.* Surface-decorated high-entropy alloy catalysts with significantly boosted activity and stability. *Adv Funct Mater* 2022, **32**: 2204643.
[116] Sun HN, Song SZ, Xu XM, *et al.* Recent progress on structurally ordered materials for electrocatalysis. *Adv Energy Mater* 2021, **11**: 2101937.
[117] Linnemann J, Kanokkanchana K, Tschulik K. Design strategies for electrocatalysts from an electrochemist's perspective. *ACS Catal* 2021, **11**: 5318–5346.
[118] Meyer Q, Yang CJ, Cheng Y, *et al.* Overcoming the electrode challenges of high-temperature proton exchange membrane fuel cells. *Electrochem Energy Rev* 2023, **6**: 16.
[119] Yin PF, Zhou M, Chen JZ, *et al.* Synthesis of palladium-based crystalline@amorphous core-shell nanoplates for highly efficient ethanol oxidation. *Adv Mater* 2020, **32**: 2000482.
[120] Joo J, Kim T, Lee J, *et al.* Morphology-controlled metal sulfides and phosphides for electrochemical water splitting. *Adv Mater* 2019, **31**: 1806682.
[121] Liu D, Guo PF, Pan HG, *et al.* Emerging high-entropy compounds for electrochemical energy storage and conversion. *Prog Mater Sci* 2024, **145**: 101300.
[122] Li XY, Rong HP, Zhang JT, *et al.* Modulating the local coordination environment of single-atom catalysts for enhanced catalytic performance. *Nano Res* 2020, **13**: 1842–1855.
[123] Luo X, Ji PX, Wang PY, *et al.* Interface engineering of hierarchical branched Mo-doped Ni_3S_2/Ni_xP_y hollow heterostructure nanorods for efficient overall water splitting. *Adv Energy Mater* 2020, **10**: 1903891.
[124] Badalyan A, Stahl SS. Cooperative electrocatalytic alcohol oxidation with electron-proton-transfer mediators. *Nature* 2016, **535**: 406–410.
[125] Liu HL, Nosheen F, Wang X. Noble metal alloy complex nanostructures: Controllable synthesis and their electrochemical property. *Chem Soc Rev* 2015, **44**: 3056–3078.
[126] Yao YG, Dong Q, Brozena A, *et al.* High-entropy nanoparticles: Synthesis–structure–property relationships and data-driven discovery. *Science* 2022, **376**: eabn3103.
[127] Xie H, Chen SQ, Liang JS, *et al.* Weakening intermediate bindings on CuPd/Pd core/shell nanoparticles to achieve Pt-like bifunctional activity for hydrogen evolution and oxygen reduction reactions. *Adv Funct Mater* 2021, **31**: 2100883.
[128] Wang Y, Gong N, Liu HF, *et al.* Ordering-dependent hydrogen evolution and oxygen reduction electrocatalysis of high-entropy intermetallic $Pt_4FeCoCuNi$. *Adv Mater* 2023, **35**: 2302067.
[129] Wei M, Sun YY, Zhang JY, *et al.* High-entropy alloy nanocrystal assembled by nanosheets with d–d electron interaction for hydrogen evolution reaction. *Energ Environ Sci* 2023, **16**: 4009–4019.
[130] Kwon J, Sun S, Choi S, *et al.* Tailored electronic structure of Ir in high entropy alloy for highly active and durable bifunctional electrocatalyst for water splitting under an acidic environment. *Adv Mater* 2023, **35**: 2300091.
[131] Chen Q, Han X, Xu ZY, *et al.* Atomic phosphorus induces tunable lattice strain in high entropy alloys and boosts alkaline water splitting. *Nano Energy* 2023, **110**: 108380.
[132] Zhang XY, Yang YY, Liu YJ, *et al.* Defect engineering of a high-entropy metallic glass surface for high-performance overall water splitting at ampere-level current densities. *Adv Mater* 2023, **35**: 2303439.
[133] Liu H, Qin HY, Kang JL, *et al.* A freestanding nanoporous NiCoFeMoMn high-entropy alloy as an efficient electrocatalyst for rapid water splitting. *Chem Eng J* 2022, **435**: 134898.
[134] Kang YQ, Cretu O, Kikkawa J, *et al.* Mesoporous multimetallic nanospheres with exposed highly entropic alloy sites. *Nat Commun* 2023, **14**: 4182.
[135] Maulana AL, Chen PC, Shi ZX, *et al.* Understanding the structural evolution of IrFeCoNiCu high-entropy alloy nanoparticles under the acidic oxygen evolution reaction. *Nano Lett* 2023, **23**: 6637–6644.
[136] Li R, Liu XJ, Liu WH, *et al.* Design of hierarchical porosity via manipulating chemical and microstructural complexities in high-entropy alloys for efficient water electrolysis. *Adv Sci* 2022, **9**: 2105808.
[137] Huang K, Xia JY, Lu Y, *et al.* Self-reconstructed spinel surface structure enabling the long-term stable hydrogen evolution reaction/oxygen evolution reaction efficiency of FeCoNiRu high-entropy alloyed electrocatalyst. *Adv Sci* 2023, **10**: 2300094.
[138] Li YZ, Tang JL, Zhang HL, *et al. In-situ* construction and repair of high catalytic activity interface on corrosion-resistant high-entropy amorphous alloy electrode for hydrogen production in high-temperature dilute sulfuric acid electrolysis. *Chem Eng J* 2023, **453**: 139905.
[139] Zhu H, Zhu ZF, Hao JC, *et al.* High-entropy alloy stabilized active Ir for highly efficient acidic oxygen evolution. *Chem Eng J* 2022, **431**: 133251.
[140] Jia Z, Yang T, Sun LG, *et al.* A novel multinary intermetallic as an active electrocatalyst for hydrogen evolution. *Adv Mater* 2020, **32**: 2000385.
[141] Chen ZJ, Zhang T, Gao XY, *et al.* Engineering microdomains of oxides in high-entropy alloy electrodes toward efficient oxygen evolution. *Adv Mater* 2021, **33**: 2101845.
[142] Wang SQ, Xu BL, Huo WY, *et al.* Efficient FeCoNiCuPd thin-film electrocatalyst for alkaline oxygen and hydrogen evolution reactions. *Appl Catal B Environ* 2022, **313**: 121472.
[143] Fu XB, Zhang JH, Zhan SQ, *et al.* High-entropy alloy nanosheets for fine-tuning hydrogen evolution. *ACS Catal* 2022, **12**: 11955–11959.
[144] Zhang D, Shi Y, Zhao H, *et al.* The facile oil-phase synthesis of a multi-site synergistic high-entropy alloy to promote the alkaline hydrogen evolution reaction. *J Mater Chem A* 2021, **9**: 889–893.
[145] Raja DS, Ting YC, Lin TY, *et al.* Quad-metallic MOF-derived carbon-armored pseudo-high entropy alloys as a bifunctional electrocatalyst for alkaline water electrolysis at high current densities. *J Mater Chem A* 2023, **11**: 25283–25297.
[146] Chang SQ, Cheng CC, Cheng PY, *et al.* Pulse electrodeposited FeCoNiMnW high entropy alloys as efficient and stable bifunctional electrocatalysts for acidic water splitting. *Chem Eng J* 2022, **446**: 137452.
[147] Chen ZQ, Wen JB, Wang CH, *et al.* Convex cube-shaped $Pt_{34}Fe_5Ni_{20}Cu_{31}Mo_9Ru$ high entropy alloy catalysts toward high-performance multifunctional electrocatalysis. *Small* 2022, **18**: 2204255.
[148] Abdelhafiz A, Wang BM, Harutyunyan AR, *et al.* Carbothermal shock synthesis of high entropy oxide catalysts: Dynamic structural and chemical reconstruction boosting the catalytic activity and stability toward oxygen evolution reaction. *Adv Energy Mater* 2022, **12**: 2200742.
[149] He YT, Zhu XH, Zhang CX, *et al.* Self-circulating adsorption–desorption structure of non-noble high-entropy alloy electrocatalyst facilitates efficient water splitting. *ACS Sustain Chem Eng* 2023, **11**: 5055–5064.
[150] Li HD, Sun MZ, Pan Y, *et al.* The self-complementary effect through strong orbital coupling in ultrathin high-entropy alloy nanowires boosting pH-universal multifunctional electrocatalysis. *Appl Catal B Environ* 2022, **312**: 121431.
[151] Hu C, Yue KH, Han JJ, *et al.* Misoriented high-entropy iridium ruthenium oxide for acidic water splitting. *Sci Adv* 2023, **9**: adf9144.

[152] Sivanantham A, Lee H, Hwang SW, *et al.* Complementary functions of vanadium in boosting electrocatalytic activity of CuCoNiFeMn high-entropy alloy for water splitting. *Adv Funct Mater* 2023, **33**: 2301153.
[153] Wu H, Lu Q, Li YJ, *et al.* Structural framework-guided universal design of high-entropy compounds for efficient energy catalysis. *J Am Chem Soc* 2023, **145**: 1924–1935.
[154] Shaikh JS, Rittiruam M, Saelee T, *et al.* First-principles and experimental insight of high-entropy materials as electrocatalysts for energy-related applications: Hydrogen evolution, oxygen evolution, and oxygen reduction reactions. *Mater Sci Eng R Rep* 2024, **160**: 100813.
[155] Domínguez-Saldaña A, Navarrete L, Balaguer M, *et al.* Enhanced hydrogen production in microwave-driven water-splitting redox cycles by engineering ceria properties. *Adv Energy Mater* 2024, **14**: 2401443.
[156] Yang YY, Jia Z, Zhang XY, *et al.* Chemical short-range order in multi-principal element alloy with ordering effects on water electrolysis performance. *Mater Today* 2024, **72**: 97–108.
[157] Ma DW, Jia YS, Li Y, *et al.* Anion modulate the morphological and electronic structure of NiFe-based electrocatalyst for efficient urea oxidation-assisted water electrolysis. *J Mater Sci Technol* 2024, **197**: 207–214.
[158] Liu ZW, Ai J, Sun MM, *et al.* Phosphorous-doped graphite layers with outstanding electrocatalytic activities for the oxygen and hydrogen evolution reactions in water electrolysis. *Adv Funct Mater* 2020, **30**: 1910741.
[159] Lv XW, Tian WW, Yuan ZY. Recent advances in high-efficiency electrocatalytic water splitting systems. *Electrochem Energy Rev* 2023, **6**: 23.
[160] Yang XX, Liang JS, Shi QR, *et al.* Regulating the third metal to design and engineer multilayered NiFeM (M: Co, Mn, and Cu) nanofoam anode catalysts for anion-exchange membrane water electrolyzers. *Adv Energy Mater* 2024, **14**: 2400029.
[161] Lee SJ, Theerthagiri J, Nithyadharseni P, *et al.* Heteroatom-doped graphene-based materials for sustainable energy applications: A review. *Renew Sust Energ Rev* 2021, **143**: 110849.
[162] Wang J, Pan FW, Chen WM, *et al.* Pt-based intermetallic compound catalysts for the oxygen reduction reaction: Structural control at the atomic scale to achieve a win–win situation between catalytic activity and stability. *Electrochem Energy Rev* 2023, **6**: 6.
[163] Fang L, Xie YP, Guo PY, *et al. In situ* formation of highly exposed $NiPS_3$ nanosheets on nickel foam as an efficient 3D electrocatalyst for overall water splitting. *Sustainable Energy Fuels* 2021, **5**: 2537–2544.
[164] Chen XJ, Li W, Reed D, *et al.* On energy storage chemistry of aqueous Zn-ion batteries: From cathode to anode. *Electrochem Energy Rev* 2023, **6**: 33.
[165] Wang YZ, Zhang XY, He HJ, *et al.* Ordered mesoporous high-entropy intermetallics for efficient oxygen reduction electrocatalysis. *Adv Energy Mater* 2024, **14**: 2303923.
[166] Wang XL, Ma RG, Li SL, *et al. In situ* electrochemical oxyanion steering of water oxidation electrocatalysts for optimized activity and stability. *Adv Energy Mater* 2023, **13**: 2300765.
[167] Jiang B, Ban XH, Wang Q, *et al.* Anionic P-substitution toward ternary Ni–S–P nanoparticles immobilized graphene with ultrahigh rate and long cycle life for hybrid supercapacitors. *J Mater Chem A* 2019, **7**: 24374–24388.
[168] Yu ZP, Boukhvalov DW, Tan H, *et al.* Sulfur and phosphorus Co-doped FeCoNiCrMn high-entropy alloys as efficient sulfion oxidation reaction catalysts enabling self-powered asymmetric seawater electrolysis. *Chem Eng J* 2024, **494**: 153094.
[169] Li WX, Xing X, Ge RY, *et al.* Electronic optimization of heterostructured MoS_2/Ni_3S_2 by P doping as bifunctional electrocatalysts for water splitting. *Sustain Mater Technol* 2023, **38**: 00743.
[170] Wang B, Tang C, Wang HF, *et al.* Anion-regulated hydroxysulfide monoliths as OER/ORR/HER electrocatalysts and their applications in self-powered electrochemical water splitting. *Small Meth* 2018, **2**: 1800055.
[171] Chen J, Wang KX, Liu ZM, *et al.* Sulfurization-induced lattice disordering in high-entropy catalyst for promoted bifunctional electro-oxidation behavior. *Chem Eng J* 2024, **489**: 151234.
[172] Huang SC, Meng YY, He SM, *et al.* N-, O-, and S-tridoped carbon-encapsulated Co_9S_8 nanomaterials: Efficient bifunctional electrocatalysts for overall water splitting. *Adv Funct Mater* 2017, **27**: 1606585.
[173] Jo S, Kim MC, Lee KB, *et al.* Nonprecious high-entropy chalcogenide glasses-based electrocatalysts for efficient and stable acidic oxygen evolution reaction in proton exchange membrane water electrolysis. *Adv Energy Mater* 2023, **13**: 2301420.
[174] Liu CC, Gong T, Zhang J, *et al.* Engineering Ni_2P–$NiSe_2$ heterostructure interface for highly efficient alkaline hydrogen evolution. *Appl Catal B Environ* 2020, **262**: 118245.
[175] Dong KX, Tran DT, Li X, *et al.* Three-phase interface engineering via P-doped $CoMo_2S_4$-integrated $Co4_S3/Co_2P$ enables high-efficiency overall water splitting. *Appl Catal B Environ Energy* 2024, **344**: 123649.
[176] Wang XL, Kim EM, Senthamaraikannan TG, *et al.* Porous hollow high entropy metal oxides $(NiCoCuFeMg)_3O_4$ nanofiber anode for high-performance lithium-ion batteries. *Chem Eng J* 2024, **484**: 149509.
[177] Xu C, Zhong SD, Yuan L, *et al.* Insight into the promotional effect of Ce doped in $(FeCoNiCrMn)_3O_4$ high entropy oxides for solvent-free aerobic oxidation of benzyl alcohol. *Chem Eng J* 2024, **481**: 148767.
[178] Li LG, Wang PT, Shao Q, *et al.* Metallic nanostructures with low dimensionality for electrochemical water splitting. *Chem Soc Rev* 2020, **49**: 3072–3106.
[179] Hu JN, Tian LC, Wang HY, *et al.* Theoretical screening of single-atom electrocatalysts of MXene-supported 3d-metals for efficient nitrogen reduction. *Chinese J Catal* 2023, **52**: 252–262.
[180] Wu DS, Kusada K, Nanba Y, *et al.* Noble-metal high-entropy-alloy nanoparticles: Atomic-level insight into the electronic structure. *J Am Chem Soc* 2022, **144**: 3365–3369.
[181] Hu J, Guo TQ, Zhong XY, *et al. In situ* reconstruction of high-entropy heterostructure catalysts for stable oxygen evolution electrocatalysis under industrial conditions. *Adv Mater* 2024, **36**: 2310918.
[182] Zhu H, Sun SH, Hao JC, *et al.* A high-entropy atomic environment converts inactive to active sites for electrocatalysis. *Energy Environ Sci* 2023, **16**: 619–628.
[183] Li WY, Zhao ZX, Zhao JY, *et al.* High entropy $La(Cr_{0.2}Mn_{0.2}Fe_{0.2}Co_{0.2}Ni_{0.2})O_3$ with tailored e g occupancy and transition metal-oxygen bond properties for oxygen reduction reaction. *J Mater Sci Technol* 2024, **194**: 236–246.
[184] Yi LY, Xiao SM, Wei YP, *et al.* Free-standing high-entropy alloy plate for efficient water oxidation catalysis: Structure/composition evolution and implication of high-valence metals. *Chem Eng J* 2023, **469**: 144015.
[185] Chang XJ, Zeng MQ, Liu KL, *et al.* Phase engineering of high-entropy alloys. *Adv Mater* 2020, **32**: 1907226.
[186] Tan RF, Jeong YJ, Li Q, *et al.* Defect-rich spinel ferrites with improved charge collection properties for efficient solar water splitting. *J Adv Ceram* 2023, **12**: 612–624.
[187] Zhang YQ, Liu HB, Ge RY, *et al.* Mo-induced *in situ* architecture of Ni_xCoyP/Co2P heterostructure nano-networks on nickel foam as bifunctional electrocatalysts for overall water splitting. *Sustain Mater Technol* 2022, **33**: 00461.
[188] Li T, Hu WJ, Tang CX, *et al.* Enhanced piezo-catalysis in ZnO rods with built-in nanopores. *J Adv Ceram* 2023, **12**: 2271–2283.
[189] Liu B, Zhu YT, Sha SM, *et al.* Strong interaction between

molybdenum compounds and mesoporous CMK-5 supports boosts hydrogen evolution reaction. *Adv Funct Mater* 2024, **34**: 2408613.
[190] Zhang B, Zheng YJ, Ma T, *et al.* Designing MOF nanoarchitectures for electrochemical water splitting. *Adv Mater* 2021, **33**: 2006042.
[191] Huo XR, Nie SN, Zhang YW, *et al.* Porous high-entropy alloy coatings as highly efficient electrocatalysts for electrocatalytic water splitting. *Chem Eng J* 2024, **487**: 150622.
[192] Wang CY, Zhao S, Han GQ, *et al.* Hierarchical porous nonprecious high-entropy alloys for ultralow overpotential in hydrogen evolution reaction. *Small Meth* 2024, **8**: 2301691.
[193] Xue HR, Zhang ZH, Lai Y, *et al.* Construction of Co_2P nanoparticles anchored on hollow N-doped porous carbon nanoleaf for high-efficiency water splitting. *Chem Eng J* 2024, **483**: 149057.
[194] Cui YF, Jiang SD, Fu Q, *et al.* Cost-effective high entropy core–shell fiber for stable oxygen evolution reaction at 2 $A{\cdot}cm^{-2}$. *Adv Funct Mater* 2023, **33**: 2306889.
[195] Feng G, Ning FH, Song J, *et al.* Sub-2 nm ultrasmall high-entropy alloy nanoparticles for extremely superior electrocatalytic hydrogen evolution. *J Am Chem Soc* 2021, **143**: 17117–17127.
[196] Feng G, Pan Y, Su D, *et al.* Constructing fully-active and ultra-active sites in high-entropy alloy nanoclusters for hydrazine oxidation-assisted electrolytic hydrogen production. *Adv Mater* 2024, **36**: 2309715.
[197] Gao J, Sahli F, Liu CJ, *et al.* Solar water splitting with perovskite/silicon tandem cell and TiC-supported Pt nanocluster electrocatalyst. *Joule* 2019, **3**: 2930–2941.
[198] Zeng XJ, Ye YF, Wang YQ, *et al.* Honeycomb-like MXene/$NiFeP_x$–NC with "continuous" single-crystal enabling high activity and robust durability in electrocatalytic oxygen evolution reactions. *J Adv Ceram* 2023, **12**: 553–564.
[199] Ilango PR, Savariraj AD, Huang HJ, *et al.* Electrospun flexible nanofibers for batteries: Design and application. *Electrochem Energy Rev* 2023, **6**: 12.
[200] Hu ZW, Chen KY, Zhu YH, *et al.* Synergistic effects of PtRhNiFeCu high entropy alloy nanocatalyst for hydrogen evolution and oxygen reduction reactions. *Small* 2024, **20**: 2309819.
[201] Pan MQ, Feng HY, Zhang ZY, *et al.* Observation of a robust catalyst support based on metallic glass for large current-density water electrolysis. *J Mater Chem A* 2024, **12**: 15334–15342.
[202] Zhang J, Wang G, Liao ZQ, *et al.* Iridium nanoparticles anchored on 3D graphite foam as a bifunctional electrocatalyst for excellent overall water splitting in acidic solution. *Nano Energy* 2017, **40**: 27–33.
[203] Zhang W, Xu GR, Zhang Q, *et al.* Ag@Pt core–shell icosahedral nanocrystals with solid solution interface improve pH-universal hydrogen evolution at large current densities. *Compos Part B Eng* 2023, **254**: 110600.
[204] Liu HB, Zhang YQ, Li JC, *et al.* Ultra-thin carbon layer encapsulated NiCoP coralline-like catalysts for efficient overall water electrolysis. *J Mater Chem A* 2024, **12**: 5100–5114.
[205] Shi H, Sun XY, Zeng SP, *et al.* Nanoporous nonprecious high-entropy alloys as multisite electrocatalysts for ampere-level current-density hydrogen evolution. *Small Struct* 2023, **4**: 2300042.
[206] Mo SY, Du L, Huang ZY, *et al.* Recent advances on PEM fuel cells: From key materials to membrane electrode assembly. *Electrochem Energy Rev* 2023, **6**: 28.
[207] Gao QS, Wang ZS, Gao W, *et al.* NiFeCo-based high entropy alloys nanoparticles coated with N-doped graphene layers as hydrogen evolution catalyst in alkaline solution. *Chem Eng J* 2024, **489**: 151370.
[208] Huo JJ, Ge RY, Liu Y, *et al.* Heterointerface manipulation in the architecture of Co–Mo_2C@NC boosts water electrolysis. *J Colloid Interf Sci* 2024, **655**: 963–975.
[209] Huo JJ, Ming Y, Huang XL, *et al.* Arrayed metal phosphide heterostructure by Fe doping for robust overall water splitting. *J Colloid Interf Sci* 2025, **678**: 669–681.
[210] Wang JY, Zhang JH, Hu YJ, *et al.* Activating multisite high-entropy alloy nanocrystals via enriching M-pyridinic N–C bonds for superior electrocatalytic hydrogen evolution. *Sci Bull* 2022, **67**: 1890–1897.
[211] Wang J, Gao Y, Kong H, *et al.* Non-precious-metal catalysts for alkaline water electrolysis: *operando* characterizations, theoretical calculations, and recent advances. *Chem Soc Rev* 2020, **49**: 9154–9196.
[212] Xu WB, Diesen E, He TW, *et al.* Discovering high entropy alloy electrocatalysts in vast composition spaces with multiobjective optimization. *J Am Chem Soc* 2024, **146**: 7698–7707.
[213] Wang SW, Xin HL. Predicting catalytic activity of high-entropy alloys for electrocatalysis. *Chem* 2019, **5**: 502–504.
[214] Perumal S, Han DB, Marimuthu T, *et al.* Active learning-driven discovery of sub-2 nm high-entropy nanocatalysts for alkaline water splitting. *Adv Funct Mater* 2025, **35**: 2424887.
[215] Rao ZY, Tung PY, Xie RW, *et al.* Machine learning-enabled high-entropy alloy discovery. *Science* 2022, **378**: 78–85.
[216] Kim G, Diao HY, Lee C, *et al.* First-principles and machine learning predictions of elasticity in severely lattice-distorted high-entropy alloys with experimental validation. *Acta Mater* 2019, **181**: 124–138.
[217] Ding FX, Lu YX, Chen LQ, *et al.* High-entropy strategy for electrochemical energy storage materials. *Electrochem Energy Rev* 2024, **7**: 16.
[218] Huang CL, Lin YG, Chiang CL, *et al.* Atomic scale synergistic interactions lead to breakthrough catalysts for electrocatalytic water splitting. *Appl Catal B Environ* 2023, **320**: 122016.
[219] Zhu WQ, Gao X, Yao YY, *et al.* Nanostructured high entropy alloys as structural and functional materials. *ACS Nano* 2024, **18**: 12672–12706.
[220] Hong QL, Sun B, Ai X, *et al.* Au nanocrystals modified holey PtTeAu metallene heteronanostructures for plasmon-enhanced nitrate electroreduction. *Adv Funct Mater* 2024, **34**: 2310730.
[221] Batchelor TAA, Pedersen JK, Winther SH, *et al.* High-entropy alloys as a discovery platform for electrocatalysis. *Joule* 2019, **3**: 834–845.
[222] Gao SJ, Hao SY, Huang ZN, *et al.* Synthesis of high-entropy alloy nanoparticles on supports by the fast moving bed pyrolysis. *Nat Commun* 2020, **11**: 2016.
[223] Li S, Chen BB, Wang Y, *et al.* Oxygen-evolving catalytic atoms on metal carbides. *Nat Mater* 2021, **20**: 1240–1247.